# Hidden GPCR structural transitions addressed by multiple walker supervised molecular dynamics (mwSuMD)

*Giuseppe Deganutti[1]*, Ludovico Pipitò[1], Roxana M. Rujan[1], Tal Weizmann[1], Peter Griffin[1], Antonella Ciancetta[2], Stefano Moro[3], and Christopher A. Reynolds,[1,4]**

[1] Centre for Health and Life Sciences, Coventry University, Alison Gingell Building, Coventry, CV1 5FB, UK

[2] Dipartimento di Scienze Chimiche, Farmaceutiche ed Agrarie, University of Ferrara, Via Fossato di Mortara 17/19, 44121 Ferrara, Italy

[3] Molecular Modeling Section (MMS), Dipartimento di Scienze del Farmaco, University of Padua via Marzolo 5, 35131, Padova, Italy

4 School of Life Sciences, University of Essex, Wivenhoe Park, Colchester, CO4 3SQ

*Corresponding Authors:
Giuseppe Deganutti - ad5288@coventry.ac.uk
Christopher A. Reynolds - ad5291@coventry.ac.uk

**Keywords**:
G protein-coupled receptors; G protein; binding; protein activation; molecular dynamics; supervised molecular dynamics, bitopic ligand, heterodimerization.

**Abstract**

The structural basis for the pharmacology of G protein-coupled receptors (GPCR), the most abundant membrane proteins and the target of about 35% of approved drugs, is still a matter of intense study. What makes GPCRs challenging to study is the inherent flexibility and the metastable nature of interaction with extra- and intracellular partners that drive their effects. Here, we present a molecular dynamics (MD) adaptive sampling algorithm, namely multiple walker supervised molecular dynamics (mwSuMD), to address complex structural transitions involving GPCRs without energy input. By increasing the complexity of the simulated process, we first report the binding and unbinding of the vasopressin peptide from its receptor $V_2$. Successively, we show the stimulatory ($G_s$) and inhibitory ($G_i$) G proteins binding to the adrenoreceptor $\beta_2$ ($\beta_2$ AR), and the adenosine 1 receptor ($A_1$R), respectively. Then we present the complete transition of the glucagon-like peptide-1 receptor (GLP-1R) from inactive to active, agonist and $G_s$-bound state, and the GDP release from the activated $G_s$. Finally, we report the heterodimerization between the adenosine receptor $A_2$ ($A_{2A}$R) and the dopamine receptor $D_2$ ($D_2$R) and subsequent bivalent ligand binding. We demonstrate that mwSuMD can address, without or with limited energetic bias, complex binding processes such as G protein selectivity and homo- and heterodimerization that are intrinsically linked to the dynamics of the protein and out of reach of classic MD.

## Introduction

Supervised molecular dynamics[1,2] (SuMD) is an efficient technique for studying ligand-receptor binding and unbinding pathways; here, we present the multiple walker enhancement (mwSuMD) to study a significantly wider range of structural transitions relevant to the drug design. We validated the method by applying it to G protein-coupled receptors (GPCRs), since their inherent flexibility is essential to their function and because these are the most abundant family of membrane receptors in eukaryotes[3] and the target for more than one-third of drugs approved for human use[4].

Vertebrate GPCRs are subdivided into five subfamilies (Rhodopsin or class A, Secretin or class B, Glutamate or class C, Adhesion, and Frizzled/Taste2) according to function and sequence[5,6]. X-ray and cryo-electron microscopy (cryo-EM) show that GPCRs possess seven transmembrane (TM) helices connected by three extracellular loops (ECLs) and three intracellular loops (ICLs), with an extended and structured N-terminal extracellular domain (ECD) in all subtypes, but class A. The primary function of GPCRs is transducing extracellular chemical signals into the cytosol by binding and activating four G protein families ($G_{s/olf}$, $G_{i/o}$, $G_{12/13}$, and $G_{q/11}$) responsible for decreasing ($G_{i/o}$) or increasing ($G_{s/olf}$) cyclic adenosine-3',5'-monophosphate (cAMP), and generating inositol-1,4,5-triphosphate ($IP_3$) and diacylglycerol (DAG) to increase $Ca^{2+}$ intracellular levels ($G_q$)[7].

Many aspects of GPCR pharmacology remain elusive: for example, the structural determinants of the selectivity displayed towards specific G proteins or the ability of certain agonists to drive a preferred intracellular signaling pathway over the others (i.*e.* functional selectivity or bias)[8]. GPCRs are challenging proteins to characterize experimentally due to their inherent flexibility and the transitory nature of the complexes formed with extracellular and intracellular effectors. Importantly, agonists can allosterically modify the receptor selectivity profile by imprinting unique intracellular conformations from the orthosteric binding site. The mechanism behind these phenomena is one of the outstanding questions in the GPCR field[9].

Molecular dynamics (MD) is a powerful computational methodology that predicts the movement and interactions of (bio)molecules in systems of variable complexity, at atomic detail. However, classic MD sampling is limited to the microsecond or, in the best conditions, the millisecond time scale[10,11]. For this reason, different algorithms have been designed to speed up the simulation of rare events such as ligand (un)binding and conformational transitions. Amongst the most popular and effective ones, are metadynamics[12], accelerated MD (aMD)[13], and Gaussian-accelerated MD (GaMD)[14], which introduce an energy potential to overcome the energy barriers preventing the complete exploration of the free energy surface, thus *de facto* bias the simulation. Such methods have been used to study GPCR activation[15,16]. Energetically unbiased MD protocols, on the other hand, comprise weighted ensemble MD (weMD)[17] and SuMD[1,18], which have largely been applied to (unbinding) small molecules, peptides, and small proteins[1,18–22]. Since SuMD is optimized for (un)bindings, we have designed mwSuMD to address more complex conformational transitions and protein-protein associations. GPCRs preferentially couple to very few G proteins out of 23 possible counterparts[9,23]. It is increasingly accepted that dynamic and transient interactions determine whether the encounter between a GPCR and a G protein results in productive or unproductive coupling[24]. MD simulations are considered a useful orthogonal tool for providing working hypotheses and rationalizing existing data on G protein selectivity. However, so far, it has not delivered as expected. Attempts so far have employed energetically biased simulations or have been confined to the $G\alpha$ subunit[15,16,23].

We tested mwSuMD on a series of increasingly difficult structural transitions involving both class A and class B1 GPCRs. Firstly, we validated the method on the nonapeptide arginine vasopressin (AVP) by simulating binding (dynamic docking) and unbinding paths from the vasopressin 2 receptor ($V_2R$). Dynamic docking, although more computationally demanding than standard molecular docking, provides insights into the binding mode of ligands in a fully hydrated and flexible environment. Moreover, it informs about binding paths and the complete mechanism of formation leading to an intermolecular complex, delivering in the context of binding kinetics[25] and structure-kinetics relationship (SKR) studies[26]. We then show the $G_s$ and $G_i$ G proteins binding to the adrenoreceptor $\beta_2$ ($\beta_2$ AR) and the adenosine 1 receptor ($A_1R$), respectively, starting from different conditions. GPCRs preferentially couple to very few G proteins out of 23 possible counterparts[9,23].

A further case study is the activation of the class B1 GPCR glucagon-like peptide-1 receptor (GLP-1R) by the small molecule PF06882961. GLP-1R is a validated target in type 2 diabetes and probably the best-characterized class B1 GPCR from a structural perspective. GLP-1R is the only class B1 receptor with structurally characterized non-peptidic orthosteric agonists, which makes it a model system for studying the druggability of the entire B1 subfamily. After GLP-1R agonist binding and activation, the coupling of $G_s$ and the release of GDP, which is the rate-limiting step of the G protein activation, was simulated for the first time using an energy-unbiased method.

The last GPCR key process addressed by mwSuMD is the heterodimerization in the membrane between the adenosine receptor $A_2$ ($A_{2A}R$) and the dopamine receptor $D_2$ ($D_2R$). The $A_{2A}R$:$D_2R$ heterodimer[27] is a therapeutic target for neurodegenerative diseases, Parkinson's disease, and schizophrenia[28–30] due to the reciprocal antagonistic allosteric effect between monomers[31]. $A_{2A}R$ activation reduces the binding affinity of $D_2R$ agonists, while $A_{2A}R$ antagonists enhance the dopaminergic tone by decreasing the adenosine negative allosteric modulation on $D_2R$. Heterobivalent ligands able to inhibit $A_{2A}R$ and activate $D_2R$ represent a valuable pharmacological tool[32] and, in principle, therapeutic options for conditions characterized by a reduction of dopaminergic signaling in the central nervous system. The successive dynamic docking of the heterobivalent ligand compound 26[33] to the heterodimer suggested by mwSuMD produced a ternary complex stabilized by lipids and is indicative of the usefulness of mwSuMD for illuminating the molecular events involved in GPCR function.

## Results and Discussion

### Short mwSuMD time windows improve the AVP dynamic docking prediction

Arginine vasopressin (AVP) is an endogenous hormone (**Figure S1a)** that mediates antidiuretic effects on the kidney by signaling through three class A GPCR subtypes: $V_{1a}$ and $V_{1b}$ receptors activate phospholipases via $G_{q/11}$, while the $V_2$ receptor ($V_2R$) activates adenylyl cyclase by interacting with $G_s$ [34] and is a therapeutic target for hyponatremia, hypertension, and incontinence[35]. AVP is amphipathic and in the bound state interacts with both polar and hydrophobic $V_2R$ residues located on TM helices and ECLs (**Figure S1b**). Although AVP presents an intramolecular C1-C6 disulfide bond that limits the overall conformational flexibility of the backbone, it has a high number of rotatable bonds, making dynamic docking complicated[36]. We assessed the performance of mwSuMD and the original version of SuMD in reconstructing the experimental $V_2R$:AVP complex using different settings, simulating a total of 92 binding events (**Table S1**). As a reference, the AVP RMSD during a classic (unsupervised) equilibrium MD simulation of the X-ray AVP:$V_2R$ complex was 3.80 ± 0.52 Å (**Figure S2**). SuMD[1,18] produced a minimum root mean square deviation (RMSD) to the cryo-EM complex of 4.28 Å, with most of the replicas (*i.e.,* distribution's mode) having an RMSD close to 10 Å (**Figure S3a**). mwSuMD, with the same settings (**Figure S3b, Table S1**) in terms of time window duration (600 ps), metric supervised (the distance between AVP and $V_2R$), and acceptance method (slope) produced slightly more precise results (i.e., distribution's mode RMSD = 7.90 Å) but similar accuracy (minimum RMSD = 4.60). Supervising the AVP RMSD to the experimental complex rather than the distance (**Figure S3c**) and using the SMscore (**Equation 1**) as the acceptance method (**Figure S3d**) worsened the prediction. Supervising distance and RMSD at the same time (**Figure S3e**), employing the DMscore (**Equation 2**), recovered accuracy (minimum RMSD = 4.60 Å) but not precision (distribution mode RMSD = 12.40 Å). Interestingly, decreasing the time window duration from 600 ps to 100 ps impaired the SuMD ability to predict the experimental complex (**Figure 1a**), but enhanced mwSuMD accuracy and precision (**Figure 1b-d**). The combination of RMSD as the supervised metric and SMscore produced the best results in terms of minimum RMSD and distribution mode RMSD, 3.85 Å and 4.40 Å, respectively (**Figure 1d, Video S1**), in agreement with the AVP deviations in the equilibrium MD simulation of the X-ray AVP:$V_2R$ complex (**Figure S2**)**.** These results confirm the inherent complexity of reproducing the AVP:$V_2R$ complex via dynamic docking and suggest that short time windows can improve mwSuMD performance on this system. However, it is necessary to know the final bound state to employ the RMSD as the supervised metric, while the distance is required to dynamically dock ligands with unknown bound conformation as previously reported[1,23]. Both distance and RMSD-based simulations delivered insights into the binding path and the residues involved along the recognition route. For example, mwSuMD pinpointed $V_2R$ residues $E184^{ECL2}$, $P298^{ECL3}$, and $E303^{ECL3}$ (**Figure S4a**) as involved during AVP binding, although not in contact with the ligand in the orthosteric complex. None of them are yet characterized through mutagenesis studies according to the GPCRdb[37].

Further to binding, a SuMD approach was previously employed to reconstruct the unbinding path of ligands from several GPCRs[2,38]. We assessed mwSuMD's capability to simulate AVP unbinding from $V_2R$. Five mwSuMD and five SuMD replicas were collected using 100 ps time windows (**Table S1**). Overall, mwSuMD outperformed SuMD in terms of time required to complete a dissociation (**Figure S5, Video S2**), producing dissociation paths

almost 10-fold faster than SuMD**.** Such rapidity in dissociating inherently produces a limited sampling of metastable states along the pathway, which can be compensated by seeding classic (unsupervised) MD simulations from configurations extracted from the unbinding pathway[39,40]. Here, the set of $V_2R$ residues involved during the dissociation was comparable to the binding (**Figure S4b**), though ECL2 and ECL3 were slightly more involved during the association than the dissociation, in analogy with other class A and B GPCRs[20,39].

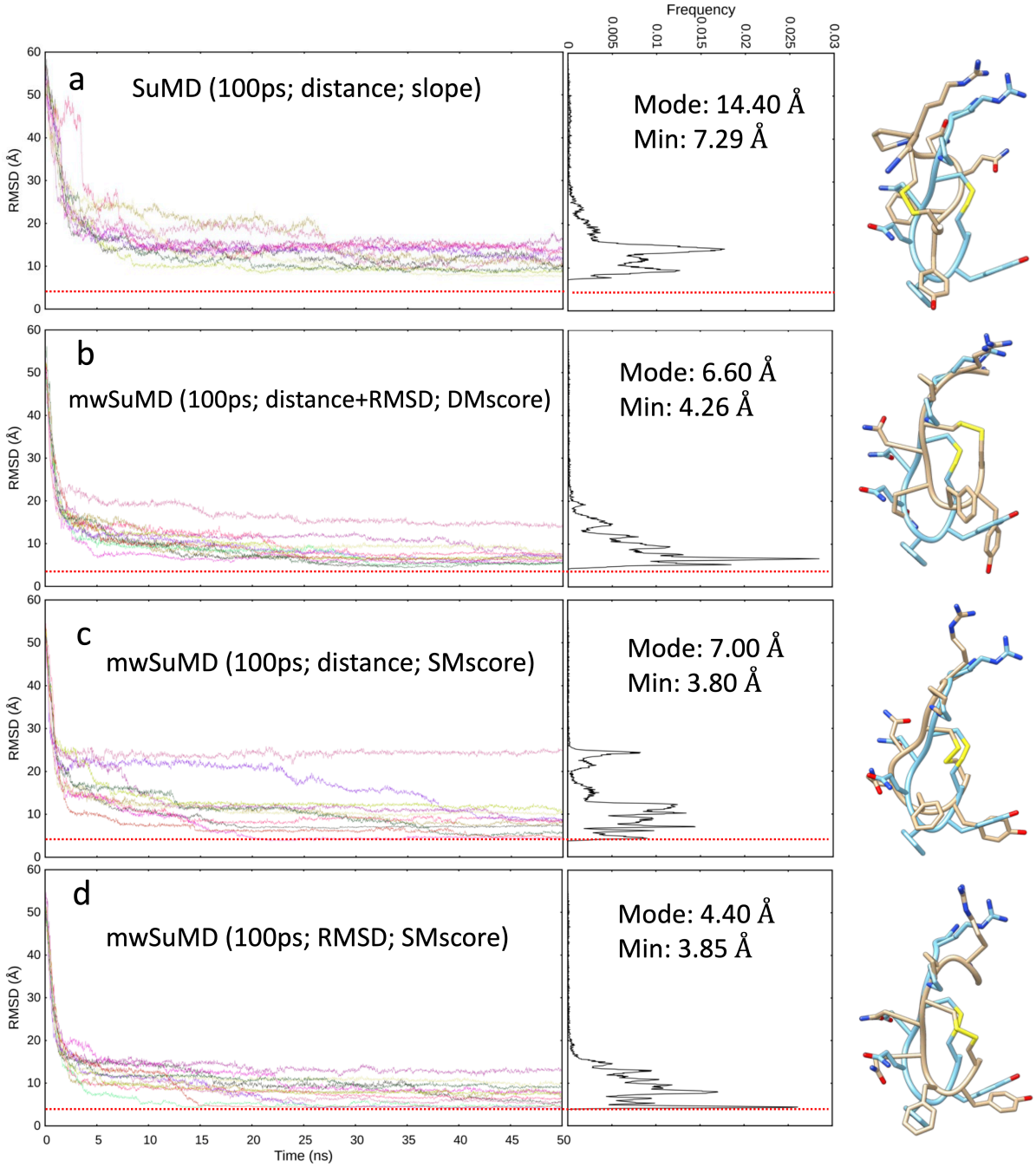


**Figure 1. AVP SuMD and mwSuMD binding simulations to $V_2R$ (100 ps time windows).** For each set of settings **(a-d)** the RMSD of AVP Cα atoms to the cryo-EM structure 7DW9 is reported during the time course of each SuMD (**a**) or mwSuMD (**b-d**) replica alongside the RMSD values distribution and

the snapshot corresponding to the lowest RMSD values (AVP from the cryo-EM structure 7DW9 is in a cyan stick representation, while AVP from simulations is in a tan stick representation). A complete description of the simulation settings is reported in Table S1 and the Methods section. The dashed red line indicates the AVP RMSD during a classic (unsupervised) equilibrium MD simulation of the X-ray AVP:$V_2$R complex (**Figure S2**).

## Binding simulations between G proteins and a class A GPCR

We tested the ability of mwSuMD to simulate the binding between a prototypical class A receptor, the $\beta_2$ adrenoreceptor ($\beta_2$ AR), and the stimulatory G protein ($G_s$), *without energy input*. mwSuMD simulations started from the intermediate, agonist-bound conformation of the $\beta_2$-AR and the inactive $G_s$ to resemble pre-coupling conditions. Three mwSuMD replicas were performed by supervising the distance between $G_s$ helix 5 ($\alpha$5) and $\beta_2$ AR as well as the RMSD of the intracellular end of TM6 to the fully active state of the receptor (**Table S1**). To monitor the progression of the simulations, we computed the RMSD of the C$\alpha$ atoms of the G$\alpha$ and G$\beta$ subunits to the experimental complex[41] (**Video S3, Figure 2ab**). During two out of three replicas, both G$\alpha$ and G$\beta$ achieved distance values close to 5 Å (minimum RMSD = 3.94 Å and 3.96 Å respectively), in good agreement with the reference (the $\beta_2$ AR:$G_s$ complex, PDB 3SN6, **Figure 2c).** The flexibility of $G_s\beta$ is backed by both MD and cryo-EM data suggesting G protein rocking motions around $G_s\alpha$:receptor interactions[20,42].

Usually, ICL3 of the GPCR and the $G_s$ protein loop hgh4, which is not found in other Gα[43], are masked out from deposited cryo-EM structures due to their high flexibility and therefore low resolution. During our simulations, these two loops formed polar intermolecular interactions through R239$^{ICL3}$, R260$^{ICL3}$, K235$^{ICL3}$, and E322$^{hgh4.12}$, D323$^{hgh4.13}$. Further transient interactions, not visible in the experiential structures, involved a mix of conserved and unique residues forming hydrogen bonds (**Table S2**): R63$^{ICL1}$-E392 $^{\alpha5.24}$, K232$^{5.71}$-D378$^{A5.10}$, K235$^{5.74}$-D378 $^{\alpha5.10}$, K235$^{ICL3}$-D343$^{H4.13}$, K267$^{6.29}$-L394$^{\alpha5}$, R239$^{ICL3}$-E314$^{hgh4.04}$, and S137$^{3.56}$-D381 $^{\alpha5.13}$. None of the interactions reported in **Table S2** is evident from the experimental $\beta_2$ AR:$G_s$ complex, implying that mwSuMD can deliver useful working hypotheses for mutagenesis and spectroscopic experiments from out-of-equilibrium simulations. Results also suggest that the $G_s$ binding is driven by a combination of conserved and unique transitory interactions with $\beta_2$ AR, possibly contributing to G protein selectivity. We speculate that the conserved interactions would be necessary for the binding, regardless of the receptor:G protein couple involved, while the transitory interactions due to the dynamics of G protein binding should produce an effective engagement of the G protein.

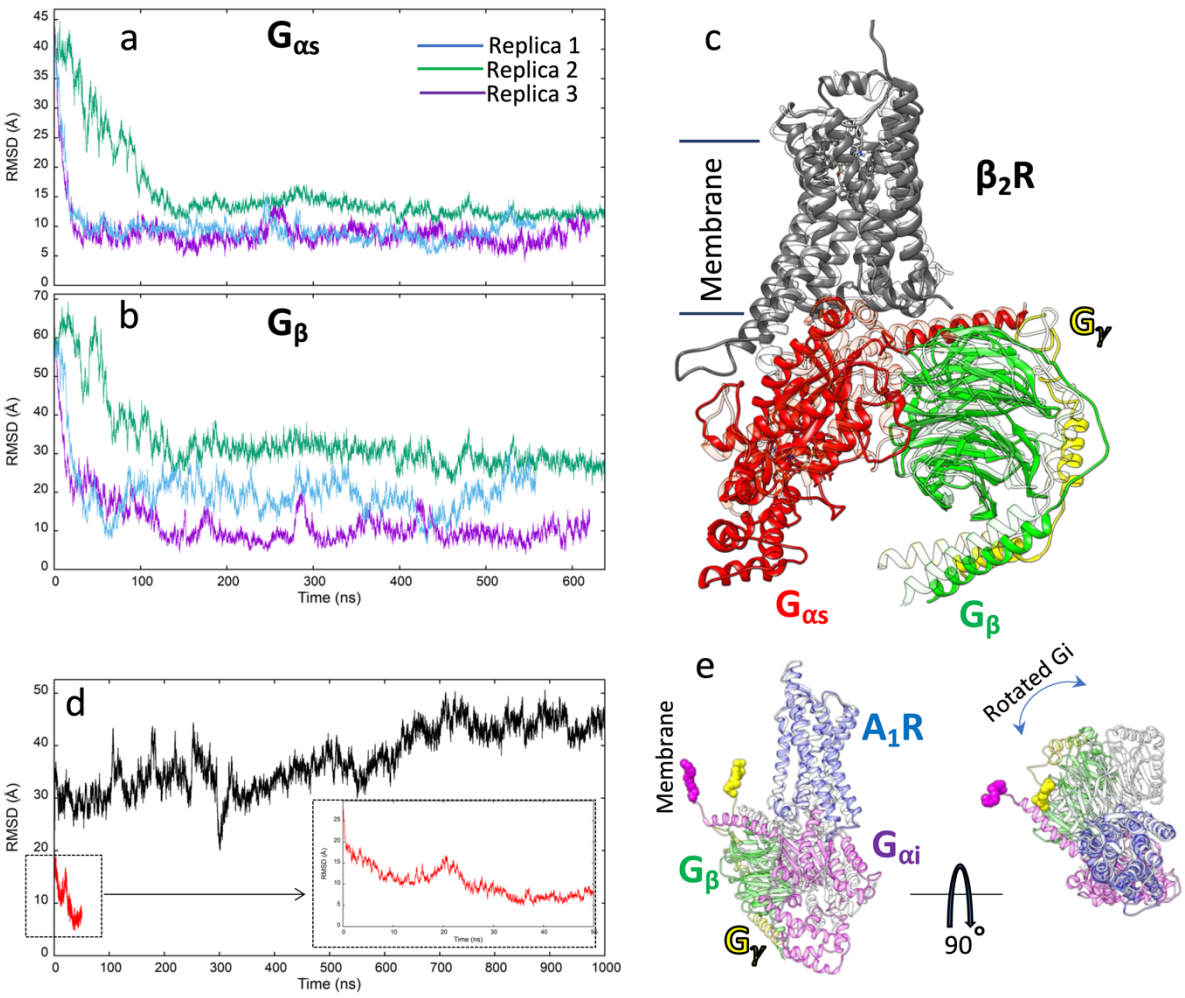


**Figure 2. G protein binding simulations to $\beta_2$AR and $A_1$R. a)** RMSD of $G_s\alpha$ to the experimental complex (PDB 3NS6) during three mwSuMD replicas; **b)** RMSD of $G_s\beta$ to the experimental complex (PDB 3NS6) during three mwSuMD replicas; **c)** superposition of the experimental $G_s$:**$\beta_2$** AR complex (transparent ribbon) and the MD frame with the lowest $G_s\alpha$ RMSD **(**3.94 Å**); d**) RMSD of $G_i\alpha$ (residues 243-355) to the $A_1$R experimental complex (PDB 6D9H) during a mwSuMD simulation (red, magnified in the box) and a 1000-ns long classic MD simulation (black); **e**) two-view superposition of the experimental $G_i$:$A_1$ R complex (transparent ribbon) and the MD frame with the lowest $G_i\alpha$ RMSD **(**4.82 Å**).**

A possible pitfall of the above-reported $G_s$:$\beta_2$ AR mwSuMD binding simulation is that G proteins bear potential palmitoylation and myristoylation sites that anchor the inactive trimer to the plasma membrane[44,45], de facto restraining possible binding paths to the receptor. Recently, the $G_i$ binding to $A_1$R was simulated by combining the biased methods GaMD with SuMD[46] but without taking into account the role played by membrane-anchoring post-translational modifications on the $G_i$ binding pathway. To address this point and test the possible system dependency of mwSuMD, we prepared a different class A GPCR, the adenosine A1 receptor ($A_1$R), and its principal effector, the inhibitory G protein ($G_i$) considering the $G_{i\alpha}$ residue C3 and $G_\gamma$ residue C65 as palmitoylated and geranylgeranylated respectively and hence inserted in the membrane. Both classic (unsupervised) and mwSuMD simulations were performed on this system for comparison (**Video S4, Figure 2d)**. In about 50 ns of mwSuMD, the $G_{i\alpha}$ subunit engaged its intracellular binding site on $A_1$R and formed a complex

in good agreement with the cryo-EM structure (PDB 6D9H, RMSD ≈ 5 Å). For comparison, 1 μs of cMD did not produce a productive engagement as the $G_{i\alpha}$ remained at RMSD values > 40 Å (**Figure 2d**), suggesting the effectiveness of mwSuMD in sampling G protein binding rare events without the input of energy. The membrane anchoring affected the overall $G_i$ binding and the final complex, which was rotated compared to the experimental structure due to the lipidation of $G_{i\alpha}$ and $G_\gamma$ (**Figure 2e)**. This suggests that future, more comprehensive studies of G protein binding and activation should consider several G protein orientations around the receptor as the starting points for mwSuMD simulations, to evaluate as many binding paths as possible

**PF06882961 binding, GLP-1R activation, and $G_s$ protein activation**

The GLP-1R has been captured by cryo-EM in both the inactive apo (ligand-free) and the active ($G_s$-bound) conformations and in complex with either peptide or non-peptide agonists[47–52]. In the inactive apo GLP-1R, residues forming the binding site for the non-peptide agonist PF06882961 are dislocated and scattered due to the structural reorganization of the transmembrane domain (TMD) and extracellular domain (ECD) (**Figure S6**) that occurs on activation. Moreover, GLP-1R in complex with GLP-1 or different agonists present distinct structural features, even amongst structurally related ligands (**Figure S7**). This complicates the scenario and suggests divergent recognition mechanisms amongst different agonists. We simulated the binding of PF06882961 using multistep supervision on different metrics of the system (**Figure 3**) to model the structural hallmark of GLP-1R activation (**Video S5**, **Video S6**).

Several metrics were supervised in a consecutive fashion. Firstly, the distance between PF06882961 and the TMD as well as the RMSD of the ECD to the active state (stage 1); secondly, the RMSD of ECD and ECL1 to the active state (stage 2); thirdly, the RMSD of PF06882961 and ECL3 to the active state (stage 3); lastly, only the RMSD of TM6 (residues I345-F367, Cα atoms) to the active state (stage 4). The combination of these supervisions produced a conformational transition of GLP-1R towards the active state (**Figure 3, Video S6**). Noteworthy, mwSuMD, like any other CV-based technique, requires some degree of knowledge of the system simulated. The sequence of these supervisions was arbitrary and does not necessarily reflect the right order of the steps involved in GLP-1R activation. This kind of planned multistep approach is feasible when the end-point receptor inactive and active structures are available, and the inherent flexibility of different domains is known. In class B GPCRs, the ECD is the most dynamic sub-structure, followed by the ECL1 and ECL3 which display high plasticity during ligand binding[20,53]. For this reason, we first supervised these elements of GLP-1R, leaving the bottleneck of activation, TM6 outward movement, as the last step. However, the protocol employed can be tweaked to study how each conformational transition takes place and influences the receptor domains. Structural elements not directly supervised, such as TM1 or TM7, displayed an RMSD reduction to the active state because they were influenced by the movement of supervised helixes or loops. For example, the supervision of ECL3 (stage 3) and TM6 (stage 4) facilitated the spontaneous rearrangement of the ECD to an active-like conformation after the ECD had previously experienced transient high flexibility during stages 2 and 3 (**Figure 3**).

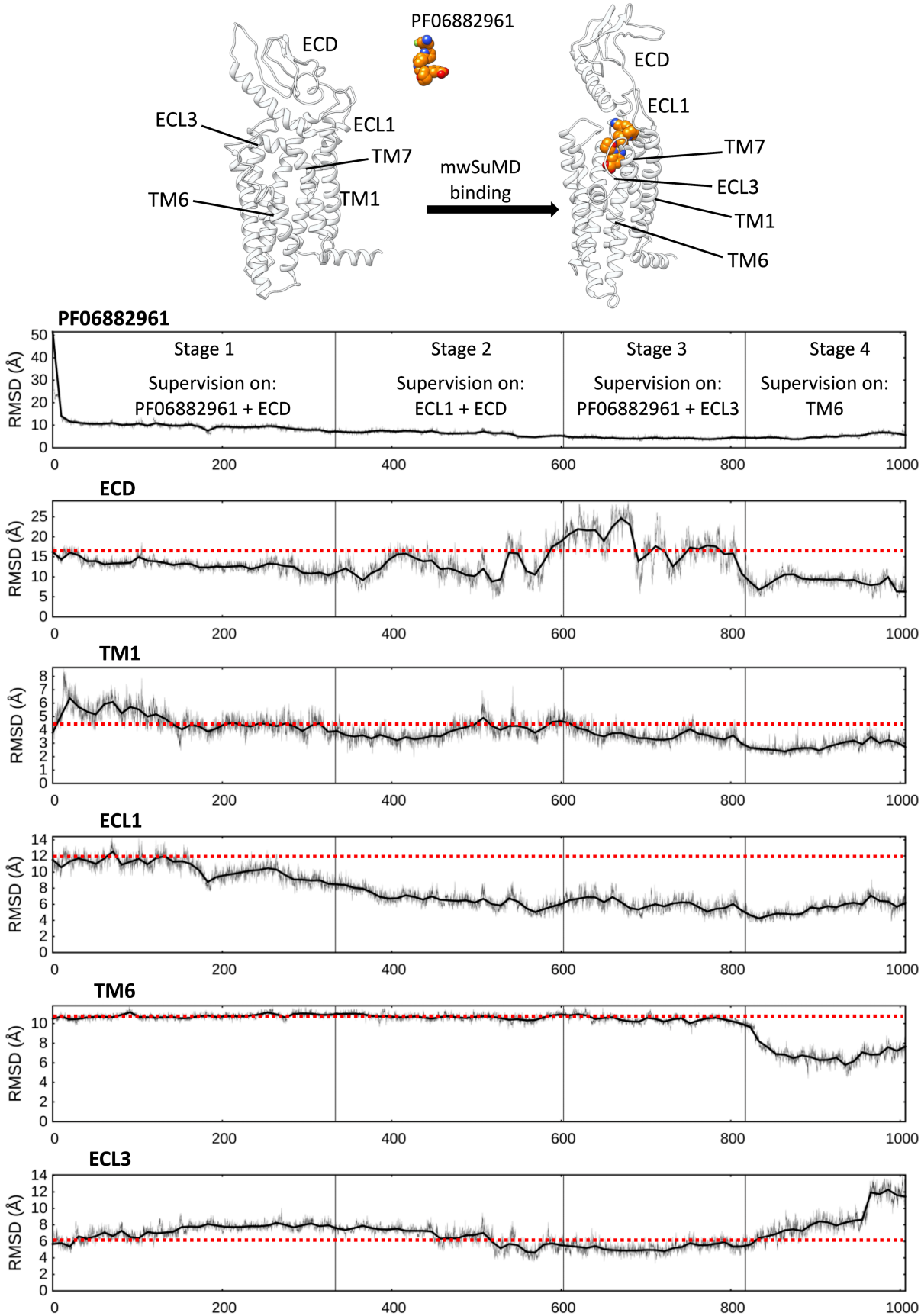
PF06882961
ECD
ECL3
ECL1
TM7
TM6
TM1
mwSuMD
binding
ECD
ECL1
TM7
ECL3
TM1
TM6
PF06882961
Stage 1
Supervision on:
PF06882961 + ECD
Stage 2
Supervision on:
ECL1 + ECD
Stage 3
Supervision on:
PF06882961 + ECL3
Stage 4
Supervision on:
TM6
ECD
TM1
ECL1
TM6
ECL3
RMSD (Å)
0
200
400
600
800
1000

**Figure 3. mwSuMD simulation of PF06882961 binding to GLP-1R and receptor activation**. Each panel reports the root mean square deviation (RMSD) to a GLP-1R structural element or the position of the ligand in the active state (top panel), over the time course (all but ECL3 converging to the active state). ECD: extracellular domain; TM: transmembrane helix; ECL: extracellular loop. The mwSuMD simulation was performed with four different settings over 1 microsecond in total. The red dashed lines show the initial RMSD value for reference.

It is worth noting that the only inactive, almost full-sequence, GLP-1R structure available, was solved with an antibody bound to the ECD. This crystallization strategy for stabilizing the receptor might have forced the ECD in a closed conformation that engages the EC *vestibule* of GLP-1R and possibly restrained the whole TMD in an altered conformation that deviates from the active conformation. This might explain why the RMSD of the TMD elements monitored during the simulation rarely reach values lower than 3 or 4 Å. During the supervision of ECL3 and PF06882961 (stage 3), we observed a loosening of the intracellular polar interactions that stabilize GLP-1R TM6 in the inactive state. As a result, the subsequent supervision of TM6 (residues I345-F367, C$\alpha$ atoms) rapidly produced the outward movement of TM6 towards the active state, in the last step of the mwSuMD simulation (stage 4). Taken together, these results suggest a concerted conformational transition for ECD and ECL1 during the binding of PF06882961 and an allosteric effect between ECL3 and the bottom of TM6. While the intracellular polar interactions were destabilized by the ECL3 transition to an active-like conformation (stages 2 and 3), the outward movement of TM6 (stage 4) did not favor the closure of ECL3 towards PF06882961, which appear to be driven by direct interactions between the ligand and R310$^{5.40}$ or R380$^{7.35}$. Interestingly, the mwSuMD simulation during Stage 4 (TM6 supervision) sampled a counterclockwise rotation of the helix (**Figure 4a**), consistent with the GLP-1R cryo-EM structures in the active, $G_s$-coupled state[50,54]. To the best of our knowledge, this is the first time an MD simulation captures the TM6 rotation upon receptor activation as results reported so far are largely limited to the TM6 opening and kinking[55].

Encouraged by results previously obtained on $G_i$ binding to $\beta_2$ AR and $A_1$R (**Figure 3**), we extracted the GLP-1R active conformation described above and simulated the $G_s$ binding to its intracellular side. Starting from the inactive, membrane-anchored $G_s$, we performed three independent mwSuMD replicas by supervising the distance between $G_s$ helix $\alpha$5 and GLP-1R residues located at the intracellular binding interface. All three mwSuMD replicas showed the $G_s$ approaching GLP-1R, with two out of three reaching an RMSD of the $G_{s\alpha}$ subunit close to or less than 10 Å, compared to the experimental complex 7LCI (**Figure 4b**). Replica 2, in particular, well reproduced the cryo-EM GLP-1R:$G_s$ complex. According to the model of G protein activation, the G protein binding has the effect of allosterically stabilizing the orthosteric agonist in complex with the receptor[56] and destabilizing the guanosine-diphosphate (GDP) bound to G$\alpha$, triggering its release and exchange with guanosine-triphosphate (GTP)[57], upon opening of the G protein alpha-helical domain (AHD). In accordance with this model, PF06882961 and GDP were respectively stabilized and destabilized during the simulated $G_s$ association (**Figure 4c,d**). The analysis of atomic contacts along the binding path of $G_s$ to GLP-1R highlights a few persistent interactions not observed in the equilibrium MD simulations of GLP-1R:$G_s$ cryo-EM complexes[56]; in particular, we propose the hidden interaction between D344$^{6.33}$ and R385 $^{\alpha 5}$ to be pivotal for $G_s$ coupling (**Table S3**).

We further investigated the $G_s$ activation mechanism by extending Replica 2 (**Figure 4b**) and supervising the opening of the $G_s$ alpha-helical domain (AHD), which is considered a necessary step to allow GDP release from the Ras-like domain[58]. We first easily obtained the opening of AHD in the extended Replica 2 and successively supervised the GDP unbinding in further three replicas, seeded after the AHD opening. In one of these three mwSuMD simulations, the nucleotide dissociated from $G_s$ (**Figure 4e-h**). **Video S7** shows the full $G_s$ binding, AHD opening, and GDP release. Interestingly, no conformational changes of the β6-α5 loop happened before or during the GDP dissociation, suggesting that its conformational change as captured in the nucleotide-free GLP-1R:$G_s$ complex (**Figure S8**) occurs after the GDP release as a result of the loss of binding stabilization, rather than being an initiator of the GDP dissociation. Our simulation is consistent with a major role played by α5 tilting and allosteric communication through internal structural elements like the β2-β3 strands, which weaken both GDP phosphate and purine binding sites as previously suggested by other groups[59–61].

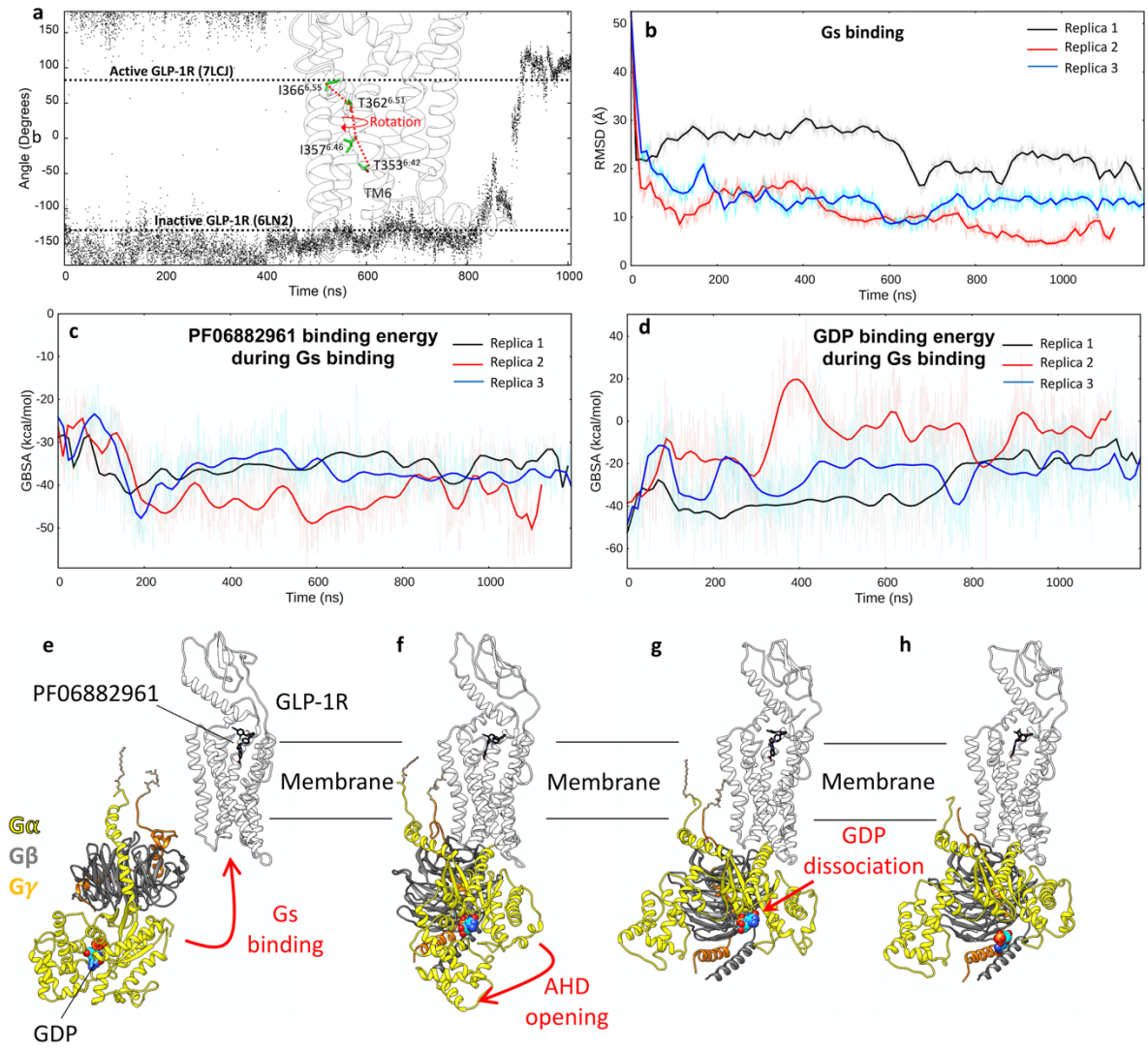


**Figure 4. GLP-1R activation and $G_s$ binding. a)** Rotation of TM6 during GLP-1R activation simulated by mwSuMD. The angle was measured as the dihedral formed by the backbone alpha carbon atoms

T353, I357, T362, and I366. The angle values of the inactive and active cryo-EM structures are reported as references; **b**) RMSD of $G_s\alpha$ to the experimental GLP-1R:$G_s$ complex (PDB 7LCJ) during three mwSuMD replicas; **c)** PF06882961 MM-GBSA binding energy during $G_s$ binding; **d**) GDP MM-GBSA binding energy during $G_s$ binding; **e-f)** sequence of simulated events during the mwSuMD $G_s$:GLP-1R simulations.

**The heterodimerization between $A_{2A}$ and $D_2R$, and binding simulations of the heterobivalent ligand compound 26.**

The current structural model of the $A_{2A}R$:$D_2R$ heterodimer is that TM4 and TM5 from both receptors contribute to the primary dimer interface, although the involvement of TM7 is not ruled out[62]. Following this interaction model, we first dynamically docked $A_{2A}R$ and $D_2R$ in an explicit 1-palmitoyl-2-oleoyl-sn-glycero-3-phosphocholine (POPC) membrane model, then simulated the binding of the heterobivalent compound 26[33] (CP26) to the preformed $A_{2A}R$:$D_2R$ heterodimer (**Video S8**). Since membrane proteins are characterized by slow lateral diffusion[63], we encouraged the encounter between $A_{2A}R$ and $D_2R$ by inputting energy using metadynamics and adiabatic MD during mwSuMD (hybrid mwSuMD/metadynamics/aMD), followed by 1.5 μs of classic MD (cMD) to relax the system and check the stability of the $A_{2A}R$:$D_2R$ interactions.

During the first 200 ns of simulation with energy bias (**Figure 5a,c** and **Figure S9a**), $A_{2A}R$ and $D_2R$ rapidly moved close to each other and reached a distance of about 30 Å (computed between centroids), before stabilizing at around 40 Å (**Figure 5a**). The computed molecular mechanics combined with the Poisson–Boltzmann and surface area continuum solvation (MM-PBSA) binding energy suggested two energy minima (**Figure 5c**) at these distances. The successive cMD simulation did not produce remarkable changes in the distance between receptors (**Figure 5b**), although the energy fluctuated before reaching about -10 kcal/mol, at the end of the simulation (**Figure 5d**). The sharp energy minima after 25 and 150 ns were due to the high number of direct contacts between $A_{2A}R$ and $D_2R$ (**Figure S9**), favored by the energy added to the system. When the input of energy bias was stopped (**Figure 5b,d**) the POPC residues re-equilibrated at the interface between proteins and mediated intracellular polar interactions between $R150^{4.40\ D2R}$, $Y146^{4.36\ D2}$ and $R199^{5.60\ A2A}$, $Y103^{3.51\ A2A}$ as well as extracellular polar interactions between the top of $TM4^{D2}$, $TM5^{D2}$ and $TM5^{A2A}$, $TM6^{A2A}$ (**Figure 5f**), suggesting that the $A_{2A}R$:$D_2R$ heterodimerization relies on lipids to mediate short-range interactions between receptors.

The dynamic docking of the heterobivalent ligand C26 further stabilized the $A_{2A}R$:$D_2R$ dimer (**Figure 5e),** in line with experimental data[33]. C26 reached the bound state rapidly, inserting the agonist pharmacophore within the $D_2R$ orthosteric site (**Figure S10, Video S8**), while the pyrazole-triazole-pyrimidine scaffold remained in a metastable complex with $A_{2A}R$, before completely binding the orthosteric site at the end of the simulation (**Figure S11, Video S8**). In the final state, the long linker between pharmacophores extended over the top of the interface formed by $A_{2A}R$ and $D_2R$ at the level of the receptors' ECL2 (**Figure 5g**). A network of polar interactions between POPC, $Y179^{A2A}$, and $Y192^{D2}$ contributed to stabilizing this ternary complex. Interestingly, the latter residues were pinpointed as important for $A_{2A}R$:$D_2R$ interactions[62]. From a binding energy perspective, C26 reached the most stable configurations between 80 and 100 ns (**Figure S12**), before the pyrazole-triazole-pyrimidine component of the ligand completed the binding to $A_{2A}R$. This suggests some contribution of the linker to the

overall stability of the ternary complex with $A_{2A}R$ and $D_2R$. Two out of four mwSuMD replicas produced $A_{2A}R$:$D_2R$:C26 ternary complexes with C26 engaged both by the orthosteric site of $A_{2A}R$ and $D_2R$, while in the remaining two replicas the $A_2AR$ pharmacophore remained stacked on the extracellular vestibule of the receptor, although in the proximity of the binding site (**Figure S10**). Considering these results, we suggest that the medicinal chemistry optimization of bivalent ligands should involve the tuning of the on-rate kinetic constant $k_{on}$ measured on each monomer of the heterodimer, to differentiate which pharmacophoric scaffold is kinetically more affected by the chemical linking and therefore aiding the surgical improvement of the bivalent ligand's affinity.

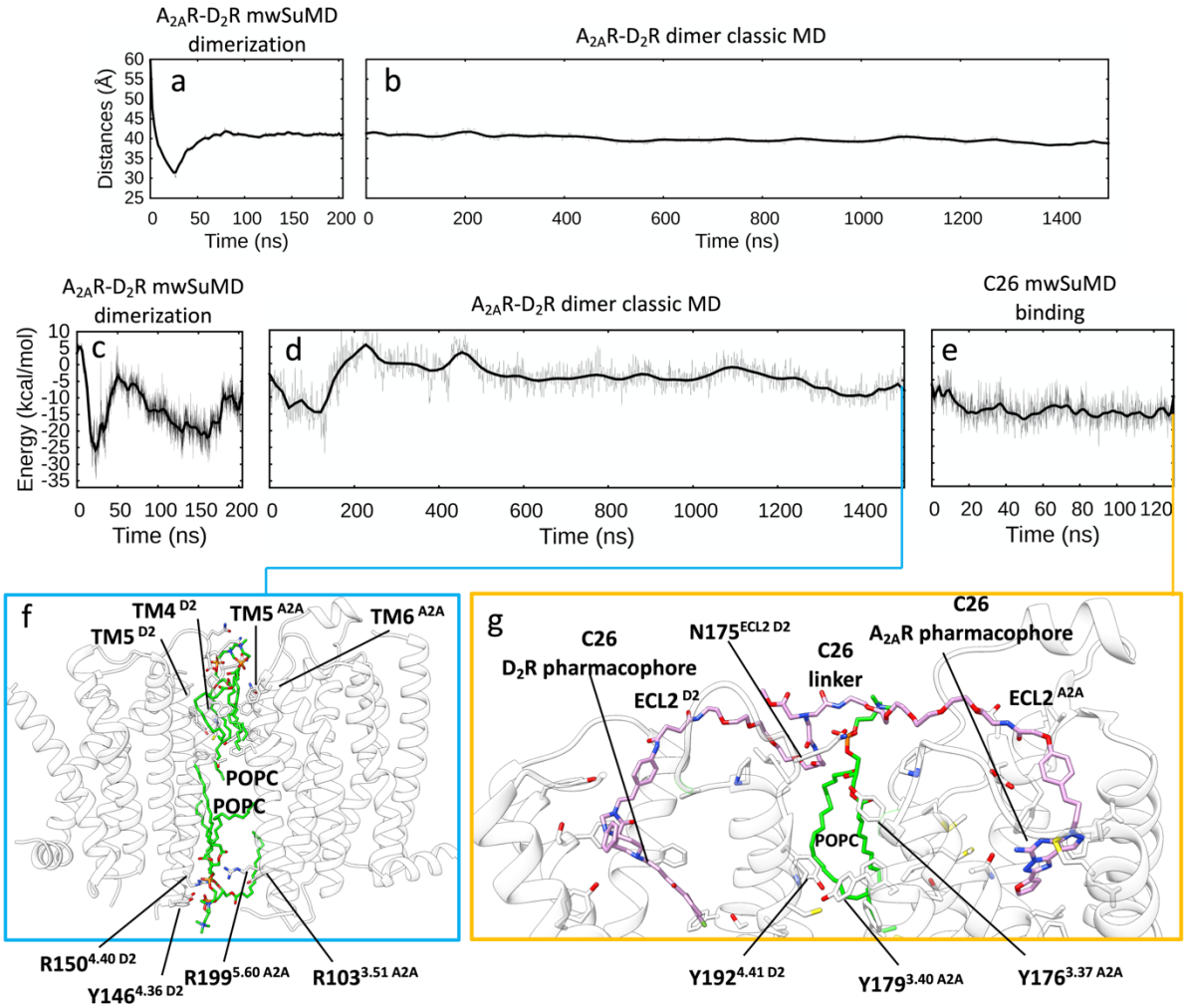


**Figure 5. $A_{2A}R$:$D_2R$ heterodimerization and formation of the ternary complex with C26. a)** Distance between the centroids of $A_{2A}R$ and $D_2R$ during the hybrid mwSuMD/metadynamics/aMD/ simulation; **b**) distance between the centroids of A2AR and D2R during the successive cMD simulation; **c**) MM-PBSA binding energy between A2AR and D2R during the hybrid metadynamics/aMD/mwSuMD simulation; **d**) MM-PBSA binding energy between A2AR and D2R during the successive cMD simulation; **e**) MM-PBSA binding energy between A2AR and D2R during the mwSuMD binding of C26. **f**) $A_{2A}R$:$D_2R$ heterodimer (white ribbon) after 1.5 μs of cMD; POPC residues (green stick) were involved in polar and hydrophobic interactions; **g**) extracellular view of the $A_{2A}R$:$D_2R$:C26 ternary complex ($D_2R$ TM2 and TM3 removed for clarity).

## Discussion

Classic MD simulations sample phase space with an efficiency that depends on the energy barrier between neighboring minima. Processes like (un)binding and protein activation require the system to overcome numerous energy barriers, some of which create bottlenecks that slows the transition down to the millisecond, or second, time scale. To overcome some of these limits, we have developed and tested on complex structural events characterizing GPCRs an energetically unbiased adaptive sampling algorithm, namely multiple walker mwSuMD, which is based on traditional SuMD, while drawing on parallel multiple replica methods[64,65],

mwSuMD performed similarly to SuMD for the dynamic docking of AVP to V2R when time windows of 600 ps were employed. Time windows of 100 ps remarkably improved mwSuMD. Usually, dynamic docking is performed to either predict the geometry of complexes or sample the binding path of an already-known intermolecular complex, or both. The RMSD of AVP to the experimental coordinates as the supervised metric produced the best results. Consequently, the RMSD should be the metric of choice to study the binding path of well-known intermolecular complexes. The distance, on the other hand, is necessary when limited structural information about the binding mode is available. In the absence of structural information regarding the final bound state, it is possible to sample numerous binding events employing mwSuMD and evaluate the final bound states rank by applying end-point free energy binding methods like the molecular mechanics energies combined with the Poisson–Boltzmann or generalized Born and surface area continuum solvation (MM/PBSA and MM/GBSA[66]) models. Our simulations propose that remarkable predictivity can be obtained with distance-driven mwSuMD, as demonstrated by the lowest deviation from the experimental AVP:V2R complex. Remarkably, the dissociation of AVP from V2R was simulated much more rapidly by mwSuMD than by SuMD, suggesting it is an efficient tool for studying the dissociation of ligands from GPCRs.

mwSuMD was further tested on the $G_s$ and $G_i$ binding to $\beta_2$ AR and $A_1$R, respectively. mwSuMD produced G protein:GPCR complexes in remarkable agreement with experimental structural data without the input of energy in a few hundred nanoseconds when starting from inactive $G_s$ and the intermediate active $\beta_2$ AR, or a few tens of nanoseconds when considering the active-state $A_1$R and $G_i$ anchored to the plasma membrane through the palmitoylation and the geranylgeranylation of $G\alpha\gamma$[44,45,67].

We increased the complexity of binding simulations by considering GLP-1R and the non-peptide agonist PF06882961. Using mwSuMD, we obtained a binding of PF06882961in good agreement with the cryo-EM structure, followed by an active-like conformational transition of GLP-1R. The choice of the metrics supervised was driven by structural data available[50] and extensive preparatory MD simulations, however, binding routes are possible from either the bulk solvent or the membrane[39,68,69]. Future studies on GLP-1R and other class B1 GPCRs should consider different starting points for the ligand and alternative apo receptor conformations to improve the sampling.

mwSuMD was able to simulate the $G_s$ binding to the active GLP-1R and the subsequent GDP release. To our knowledge, this is the first time the whole sequence of events leading from an inactive GPCR to the GDP release is simulated. Remarkably, this was obtained without biasing the simulations with external energy. Our results suggest that the full rotation and elongation of $\alpha$5 as in cryo-EM structures could occur after the GDP release, supporting the role of hidden, metastable interactions as the driving force of G protein coupling and selectivity, in accordance with recent work on GLP-1R[70].

The final case study was the dimerization process between $A_{2A}R$ and $D_2R$ in a membrane model. To speed up the encounter between receptors, we introduced an energy bias in the form of abMD and metadynamics. Although mwSuMD is an unbiased adaptive sampling method, it can be easily coupled to many forms of bias to favor the simulation of energy-requiring processes. Our results suggest a fundamental contribution of the phospholipids on the stabilization of the heterodimer, in agreement with experiments[71,72] but confuting protein-protein molecular docking results frequently predicting extended interfaces between monomers[73]. mwSuMD was able to dynamically dock the heterobivalent ligand CP26, supporting a stabilizing effect on the $A_{2A}R$:$D_2R$ heterodimer. A complete characterization of the possible interfaces between GPCR monomers, which falls beyond the goal of the present work, should be achieved by preparing different initial unbound states characterized by divergent relative orientations between monomers to dynamically dock.

mwSuMD is suited for a mechanistic description of structural events. For this reason, it well integrates with mutagenesis and kinetics experiments informed by the method, and required for the validation of its results in line with any other computational technique. We note that mwSuMD trajectories, since can describe the sequential states along a transition pathway, can represent a precious backbone for further MD sampling aimed at quantifying or predict the kinetics of the event. Approaches such as path collective variable metadynamics[74], Markov State Models[75], or machine learning models[76,77] can be informed by mwSuMD. Future work will be addressed in this direction.

In summary, we showcased the applicability domain of mwSuMD to key, but scarcely understood, aspects of GPCR structural biology, pharmacology, and drug design hitherto unaddressed by unbiased simulations. Given the generality and simplicity of its implementation, we anticipate that mwSuMD can be employed to study a wide range of structural phenomena characterizing both membrane and cytosolic proteins. mwSuMD is an ongoing project updated on https://github.com/pipitoludovico/mwSuMD_multiEngine and in the recent implementation can exploit ACEMD[78], NAMD[79], GROMACS[80] and OPENMM[81] as MD engine.

## Methods

### Multiple walker SuMD (mwSuMD) protocol

The supervised MD (SuMD) is an adaptive sampling method[82] for speeding up the simulation of binding events between small molecules (or peptides[83,84]) and proteins[1,18] without the introduction of any energetic bias. Briefly, during SuMD, a series of short unbiased MD simulations are performed, and after each simulation, the distances between the centers of mass (or the geometrical centers) of the ligand and the predicted binding site (collected at regular time intervals) are fitted to a linear function. If the resulting slope is negative (showing progress towards the target) the next simulation step starts from the last set of coordinates and velocities, otherwise, the simulation is restarted by randomly assigning the atomic velocities.

In the implementation for ACEMD used in this work, mwSuMD needs as input the initial coordinates of the system as a pdb file, the coordinates, and the atomic velocities of the system from the equilibration stage, the topology file of the system, and all the necessary force field parameters. The user can decide to supervise one (X) or two metrics (X', X'') of the simulated system over short simulations seeded in batches, called walkers. In the former case, either the slope of the linear function interpolating the metric values or a score can be adopted to decide whether to continue the mwSuMD simulation. When the user decides to supervise two metrics, then a specific score is used. In the present work, distances between centroids, RMSDs, or the number of atomic contacts between two selections were supervised (**Table S1**). The choice of the metrics is system and problem-dependent, as the RMSD is most useful when the final state is known, while the distance is required when the target state is unknown; details on the scores are given below. The decision to restart or continue mwSuMD after any short simulation is postponed until all the walkers of a batch are collected. The best short simulation is selected and extended by seeding the same number of walkers, with the same duration as the step before.

For each walker, the score for the supervision of a single metric (SMscore) is computed as the square root of the product between the metric value in the last frame ($X_{last\ frame}$) and the average metric value over the short simulation ($\bar{X}$):

$$SMscore = \sqrt{X_{last\ frame} * \bar{X}} \quad (1)$$

If the metric is set to decrease (e.g. binding or dimerization) the walker with the lowest SMscore is continued, otherwise (e.g. unbinding or outwards opening of domains), the walker with the highest score is continued. Using the SMscore rather than the slope should give more weight to the final state of each short simulation, as it is the starting point for the successive batch of simulations. Considering the average of the metric should favor short simulations consistently evolving in the desired direction along the metric.

If both X' and X'' are set to increase during the mwSuMD simulations, the score for the supervision of two metrics (DMscore) on each walker is computed as follows:

$$DMscore = \left(\left(\frac{X'_{last\ frame}}{\bar{X}'_{batch\ walkers}} - 1\right) + \left(\frac{X''_{last\ frame}}{\bar{X}''_{batch\ walkers}} - 1\right)\right) * 100 \quad (2)$$

Where $X'_{last\ frame}$ and $X''_{last\ frame}$ are the metrics values in the last frame, while $\overline{X}'_{batch\ walkers}$ and $\overline{X}''_{batch\ walkers}$ represent the average value of the two metrics over all the walkers in the batch. Subtracting the value 1 to the metric ratio ensures that if one of the two metrics from the last frame ($X'_{last\ frame}$ or $X''_{last\ frame}$) is equal to the average ($\overline{X}''_{batch\ walkers}$ or $\overline{X}''_{batch\ walkers}$) then that metric addend is null and DMscore depends only on the remaining metric. If any of the two metrics is set to decrease, then the corresponding component in Equation 2 is multiplied by -1 to maintain a positive score. Considering the average value of the two metrics over all the walkers rather than only over the considered walker should be more representative of the system evolution along the defined metric. In other words, the information about the metric is taken from all the walkers to better describe the evolution of the system.

The DMScore is designed to preserve some degree of independence between the two metrics supervised. Indeed, if the variation of one of them slows down and gets close to zero, the other metric is still able to drive the system's evolution. It should be noted that DMScore works at its best if the two metrics have similar variations over time, as in the case of distance and RMSD (both of which are distance-based). Notably, differently from SuMD, when a walker is extended by seeding a new batch of short simulations and the remaining walkers are stopped, the atomic velocities are not reassigned. This allows the simulations to be as short as a few picoseconds if desired, without introducing artifacts due to the thermostat latency to reach the target temperature (usually up to 10-20 ps when a simulation is restarted reassigning the velocities of the atoms).

The current implementation of mwSuMD is for python3 and exploits MDAnalysis[85] and MDTRaj[86] modules.

**Force field, ligands parameters, and general systems preparation**

The CHARMM36[87,88]/CGenFF 3.0.1[89–91] force field combination was employed in this work. Initial ligand force field, topology and parameter files were obtained from the ParamChem webserver[89]. Restrained electrostatic potential (RESP)[92] partial charges were assigned to all the non-peptidic small molecules but adrenaline and guanosine-5'-diphosphate (GDP) using Gaussian09 (HF/6-31G* level of theory) and AmberTools20.

Six systems were prepared for MD (**Table S1**). Hydrogen atoms were added using the pdb2pqr[93] and propka[94] software (considering a simulated pH of 7.0); the protonation of titratable side chains was checked by visual inspection. The resulting receptors were separately inserted in a 1-palmitoyl-2-oleyl-sn-glycerol-3-phosphocholine (POPC) bilayer (previously built by using the VMD Membrane Builder plugin 1.1, Membrane Plugin, Version 1.1. at: http://www.ks.uiuc.edu/Research/vmd/plugins/membrane/), through an insertion method[95]. Receptor orientation was obtained by superposing the coordinates on the corresponding structure retrieved from the OPM database[96]. Lipids overlapping the receptor transmembrane helical bundle were removed and TIP3P water molecules[97] were added to the simulation box by means of the VMD Solvate plugin 1.5 (Solvate Plugin, Version 1.5. at <http://www.ks.uiuc.edu/Research/vmd/plugins/solvate/). Finally, overall charge neutrality was reached by adding $Na^+/Cl^-$ counter ions up to the final concentration of 0.150 M), using the VMD Autoionize plugin 1.3 (Autoionize Plugin, Version 1.3. at <http://www.ks.uiuc.edu/Research/vmd/plugins/autoionize/).

**System equilibration and general MD settings**

The MD engine ACEMD3[78] was employed for both the equilibration and productive simulations. The equilibration was achieved in isothermal-isobaric conditions (NPT) using the Berendsen barostat[98] (target pressure 1 atm) and the Langevin thermostat[99] (target temperature 300 K) with low damping of 1 $ps^{-1}$. For the equilibration (integration time step of 2 fs): first, clashes between protein and lipid atoms were reduced through 1500 conjugate-gradient minimization steps, then a positional constraint of 1 kcal $mol^{-1}$ $Å^{-2}$ on all heavy atoms was gradually released over different time windows: 2 ns for lipid phosphorus atoms, 60 ns for protein atoms other than alpha carbon atoms, 80 ns for alpha carbon atoms; a further 20 ns of equilibration was performed without any positional constraints.

Productive trajectories (**Table S1**) were computed with an integration time step of 4 fs in the canonical ensemble (NVT). The target temperature was set at 300 K, using a thermostat damping of 0.1 $ps^{-1}$; the M-SHAKE algorithm[100,101] was employed to constrain the bond lengths involving hydrogen atoms. The cut-off distance for electrostatic interactions was set at 9 Å, with a switching function applied beyond 7.5 Å. Long-range Coulomb interactions were handled using the particle mesh Ewald summation method (PME)[102] by setting the mesh spacing to 1.0 Å.

**Vasopressin binding simulations**

The vasopressin 2 receptor ($V_2R$) in complex with vasopressin (AVP) and the $G_s$ protein[103] was retrieved from the Protein Data Bank[104] (PDB ID 7DW9). The $G_s$ was removed from the system and the missing residues on ECL2 (G185-G189) were modeled from scratch using Modeller 9.19[105]. AVP was placed away from $V_2R$ in the extracellular bulk and the resulting system was prepared for MD simulations and equilibrated as reported above.

During SuMD simulations, the distance between the centroids of AVP residues C1-Q4 and $V_2R$ residues Q96, Q174, Q291, and L312 (C$\alpha$ atoms only) was supervised over time windows of 600 ps or 100 ps (**Table S1**). MwSuMD simulations considered the same distance, the RMSD of AVP residues C1-Q4 to the experimental bound complex or the combination of the two during time windows of 600 ps (3 walkers) or 100 ps (10 walkers) (**Table S1**). Slope, SMscore, or DMscore (see Methods section **MwSuMD protocol**) was used in the different mwSuMD replicas performed (**Table S1**). Simulations were stopped after 300 ns (time window duration = 600 ps) or 50 ns (time window duration = 100 ps) of total SuMD or mwSuMD simulation time.

**Vasopressin unbinding simulations**

The $V_2R$:AVP complex was prepared for MD simulations and equilibrated as reported above. During both SuMD and mwSuMD simulations (**Table S1**), the distance between the centroids of AVP residues C1-Q4 and $V_2R$ residues Q96, Q174, Q291, and L312 (C$\alpha$ atoms only) was supervised over time windows of 100 ps (10 walkers seeded for mwSuMD simulations). Replicas were stopped when the AVP-$V_2R$ distance reached 40 Å.

**$G_s$ protein:$\beta_2$ AR binding simulations**

The model of the adrenergic $\beta_2$ receptor ($\beta_2$ AR) in an intermediate active state was downloaded from GPCRdb (https://gpcrdb.org/). The full agonist adrenaline (ALE) was inserted in the orthosteric site by superposition with the PDB ID 4LDO (fully active $\beta_2$ AR)[106].

The structure of the inactive, GDP-bound $G_s$ protein[107] was retrieved from the Protein Data Bank[104] (PDB ID 6EG8) and placed in the intracellular bulk. The resulting system ($G_s$ > 50 Å away from ($\beta_2$ AR) was prepared for MD simulations and equilibrated as reported above. The PDB ID 3SN6 (fully active $\beta_2$ AR in complex with $G_s$[41]) was used as the reference for RMSD computations. Three mwSuMD replicas (**Table S1**) were performed supervising at the same time the distance between the helix 5 (α5) $G_\alpha$s residues R385-L395 and the $\beta_2$ AR residues V31-P330 as well as the RMSD of $\beta_2$ AR TM6 residues C265-I278 (Cα atoms only) to the fully active state, during 100 ps time windows (5 walkers).

**Membrane-anchored Gi protein:$A_1$R simulations**

Since the full-length structure of the inactive human Gi protein has not been yet resolved by X-ray or cryo-EM, it was modeled by superimposing the AlphaFold2[108] AI models of the Gαi (P63096-F1), Gβ (Q9HAV0-F1), and Gγ (P50151-F1) subunits to the PDB file 6EG8 (a $G_s$ heterotrimer). The resulting homotrimer (without GDP) was processed through Charmm-GUI[109] to palmitoylate residue $C3^{G\alpha i}$ and geranylgeranylate residue $C65^{G\gamma}$ [44,110]. The side chains of these two lipidated residues were manually inserted into a 120 x 120 Å POPC membrane and previously built by using the VMD Membrane Builder plugin 1.1, Membrane Plugin, Version 1.1. at: http://www.ks.uiuc.edu/Research/vmd/plugins/membrane/. Lipids overlapping the palmitoyl and geranylgeranyl groups were removed and TIP3P water molecules[97] were added to the simulation box by means of the VMD Solvate plugin 1.5 (Solvate Plugin, Version 1.5. at <http://www.ks.uiuc.edu/Research/vmd/plugins/solvate/). Finally, overall charge neutrality was reached by adding $Na^+$/$Cl^-$ counter ions up to the final concentration of 0.150 M), using the VMD Autoionize plugin 1.3 (Autoionize Plugin, Version 1.3. at <http://www.ks.uiuc.edu/Research/vmd/plugins/autoionize/). The first stage of equilibration was performed as reported above (Methods section **System equilibration and general MD settings**) for 120 ns, followed by a second stage in the NVT ensemble for a further 1 μs without any restraints to allow the membrane-anchored heterotrimeric Gi protein to stabilize within the intracellular side of the simulation box. After this two-stage, long equilibration, the active state $A_1$R in complex with adenosine (PDB 6D9H) was manually inserted into the equilibrated membrane above the Gi protein using the corresponding structure retrieved from the OPM database as a reference, and the system further equilibrated for 120 ns as reported above (Methods section **System equilibration and general MD settings**). The $A_1$R-Gi system was then subjected to both a 1 μs-long classic MD simulation and a mwSuMD simulation (**Table S1**). During the mwSuMD simulation, the RMSD of helix 5 (α5) $G_\alpha$s residues 329-354 to the PDB 6D9H was supervised, seeding three walkers of 100 ps each until the productive simulation time reached 50 ns (total simulation time 150 ns).

**GLP-1R:PF06882961 binding simulations**

The inactive, ligand-free glucagon-like peptide receptor (GLP-1R) was retrieved from the Protein Data Bank[104] (PDB ID 6LN2)[111]. Missing residues in the stalk and ICL2 were modeled with Modeller 9.19. The PF06882961 initial conformation was extracted from the complex with the fully active GLP-1R[54] (PDB ID 7LCJ) and placed away from GLP-1R in the extracellular bulk. The resulting system was prepared for MD simulations and equilibrated as reported above. CGenFF dihedral force field parameters of PF06882961 with the highest penalties (dihedrals NG2R51-CG321-CG3C41-CG3C41 (penalty=143.5) and NG2R51-CG321-

CG3C41-OG3C51 (penalty=152.4)) were optimized (**Figure S13**) employing Gaussian09 (geometric optimization and dihedral scan at HF/6-31g(d) level of theory) and the VMD force field toolkit plugin[112].

Four classic MD replicas, for a total of 8 μs, were performed on the inactive, ligand-free receptor (prepared for MD simulations and equilibrated as reported above) to assess the possible binding path to the receptor TMD and therefore decide the initial position of PF06882961 in the extracellular bulk of the simulation box. A visual inspection of the trajectories suggested three major conformational changes that could allow ligand access to the TMD (**Figure S13**). Transitory openings of the ECD (distance $Q47^{ECD}$ - $S310^{ECL2}$), TM6-TM7 (distance $H363^{6.52}$ - $F390^{7.45}$), and TM1-ECL1 (distance $E138^{1.33}$ and $W214^{ECL1}$) were observed. Since the opening of TM1-ECL1 was observed in two replicas out of four, we placed the ligand in a favorable position for crossing that region of GLP-1R.

MwSuMD simulations (**Table S1**) were performed stepwise to dock the ligand within GLP-1R first and then relax the receptor towards the active state. The PF06882961 binding was obtained by supervising at the same time the distance between the ligand and GLP-1R TM7 residues $L379^{7.34}$-$F381^{7.36}$, which are part of the orthosteric site (Cα atoms only), and the RMSD of the ECD (residues $W33^{ECD}$-$W120^{ECD}$, Cα atoms only) to the active state (PDB ID 7LCJ) until the former distance reached 4 Å. In the second phase of mwSuMD, the RMSD of the ECD (residues $W33^{ECD}$-$W120^{ECD}$, Cα atoms only) and the ECL1 to the active state (PDB ID 7LCJ) Cα atoms of residues $M204^{2.74}$-$L224^{3.27}$) were supervised until the latter reached less than 4 Å. During the third phase, the RMSD of PF06882961, as well as the RMSD of ECL3 (residues $A368^{6.57}$-$T378^{7.33}$, Cα atoms), were supervised until the former reached values lower than 3 Å. In the last mwSuMD step, only the RMSD of TM6 (residues $I345^{6.34}$-$F367^{6.56}$, Cα atoms) to the active state (PDB ID 7LCJ) was supervised until less than 5 Å.

**Membrane-anchored $G_s$ protein:GLP-1R simulations and GDP dissociation.**

The PDB 6EG8 was processed through Charmm-GUI[109] to palmitoylate residue $C3^{G\alpha i}$. The Gβ and Gγ subunits prepared as reported above were superimposed to the PDB file 6EG8 and the original Gβ and Gγ were removed. This step produced a heterotrimeric $G_s$ protein palmitoylated at residue $C3^{G\alpha s}$ and geranylgeranylated at residue $C65^{G\gamma}$. The resulting system was inserted into a 120 x 120 Å POPC membrane and previously built by using the VMD Membrane Builder plugin 1.1, Membrane Plugin, Version 1.1. at: http://www.ks.uiuc.edu/Research/vmd/plugins/membrane. Lipids overlapping the palmitoyl and geranylgeranyl groups were removed and TIP3P water molecules[97] were added to the simulation box by means of the VMD Solvate plugin 1.5 (Solvate Plugin, Version 1.5. at <http://www.ks.uiuc.edu/Research/vmd/plugins/solvate/). Finally, overall charge neutrality was reached by adding $Na^+$/$Cl^-$ counter ions up to the final concentration of 0.150 M), using the VMD Autoionize plugin 1.3 (Autoionize Plugin, Version 1.3. at <http://www.ks.uiuc.edu/Research/vmd/plugins/autoionize/). The first stage of equilibration was performed as reported above (Methods section **System equilibration and general MD settings**) for 120 ns, followed by a second stage in the NVT ensemble for a further 1 μs without any restraints to allow the membrane-anchored heterotrimeric $G_s$ protein to stabilize within the intracellular side of the simulation box. After this two-stage long equilibration, GLP-1R from the final frame of the activation simulation (in complex with PF06882961) was manually inserted into the equilibrated membrane above the $G_s$ protein using the corresponding

structure retrieved from the OPM database as a reference, and the system further equilibrated for 120 ns as reported above (Methods section **System equilibration and general MD settings**). The GLP-1R-$G_s$ system was then subjected to three simulations (**Table S1**). Each mwSuMD replica was interrupted by 500 ns of classic MD twice, to relax the system during the transition. In the supervised stages, the distance between residues M386-L394 $^{G\alpha s}$ of helix 5 (α5) and the GLP-1R intracellular residues R176$^{2.46}$, R348$^{6.37}$, S352$^{6.41}$, and N405$^{7.60}$ was monitored, seeding three walkers of 200 ps each.

The AHD opening was simulated starting from the best GLP-1R:$G_s$ binding mwSuMD replica (Replica 2 in **Figure 4**) by supervising the distance between AHD residues G70-R199 $^{G\alpha s}$ and K300-L394$^{G\alpha s}$ during three walkers of 100 ps each. 300 ns of classic MD was performed to relax the system. Finally, the GDP unbinding was supervised as the distance between GDP and residues E50, K52, T55, K293, and V367 of $G_{\alpha s}$; five walkers were used in a 50 ps long mwSuMD simulation.

**A2A:D2R heterodimerization**

The inactive state $A_{2A}R$ and $D_2R$ were retrieved from the Protein Data Bank[104] (PDB 5NM4 and 6LUQ, respectively)[113,114]. Antagonists bound to the orthosteric site were removed and no modeling of the missing IC loops was attempted. $A_{2A}R$ and $D_2R$ were manually placed roughly 40 Å away from each other, on the plane of the membrane, orienting the two receptors to favor the dimerization through the interface formed by TM4 and TM5, as suggested by Borroto-Esquela D. O. *et al*.[62] The resulting system was prepared for MD simulations and equilibrated as reported above.

The heterodimerization between $A_{2A}R$ and $D_2R$ was simulated with mwSuMD, seeding batches of three walkers with a duration of 100 ps each (**Table S1).** During each walker, the distance between TM5 of $A_{2A}R$ and $D_2R$ was supervised. At the same time, the distance between the centroids of $A_{2A}R$ and $D_2R$ was used as a collective variable for adiabatic MD[115] (abMD) and well-tempered metadynamics[116,117] (wtMetaD) performed with Plumed 2.6[118]. For abMD, a distance target of 30 Å and a force constant of 10000 kJ*mol$^{-1}$*Å$^{-1}$) was used, while wtMetaD was performed by seeding Gaussian functions every 1 ps (sigma=1 Å; height=0.837 kJ*mol$^{-1}$; T=310K) with a bias factor of 30. When the $A_{2A}R$ - $D_2R$ distance reached values lower than 40 Å and the first contacts between proteins were formed, the abMD was stopped and wtMetaD continued with a harmonic energy wall at 30 Å to avoid artificial crushing between the receptors due to the added energy bias. When the distance between $A_{2A}R$ and $D_2R$ was stable at about 30 Å, the collective variable biased by wtMetaD was set as the number of atomic contacts between $A_{2A}R$ and $D_2R$, until reaching 200 ns of simulation. Finally, to relax the system and challenge the stability of the heterodimer formed during the biased mwSuMD simulation, a 1.5 μs classic MD simulation was performed.

**$A_{2A}R$-$D_2R$ heterobitopic ligand binding simulations**

The $A_2AR$-$D_2R$ heterobivalent ligand compound 26[33] was parameterized as reported above and placed in the bulk solvent of the $A_2AR$:$D_2R$ complex from the classic MD. Four mwSuMD replicas were collected supervising at the same time the distance between the $A_{2A}$ antagonist pyrazole-triazole-pyrimidine scaffold and the centroid of $A_{2A}R$ residues F168, N253, and A277 (Cα atoms) as well as the distance between the $D_2$ antagonist 4-fluorobenzyl scaffold and the centroids of the Cα of $D_2R$ residues C118, F198, and V115 (Cα atoms). Ten walkers of 100 ps were simulated for every mwSuMD batch of replicas.

**MD Analysis**

Interatomic distances were computed through MDAnalysis[85]; root mean square deviations (RMSD) were computed using VMD[119] and MDAnalysis[85].

Interatomic contacts and ligand-protein hydrogen bonds were detected using the GetContacts scripts tool (https://getcontacts.github.io), setting a hydrogen bond donor-acceptor distance of 3.3 Å and an angle value of 120° as geometrical cut-offs. Contacts and hydrogen bond persistency are quantified as the percentage of frames (over all the frames obtained by merging the different replicas) in which protein residues formed contacts or hydrogen bonds with the ligand.

The MMPBSA.py[120] script, from the AmberTools20 suite (The Amber Molecular Dynamics Package, at http://ambermd.org/), was used to compute molecular mechanics energies combined with the generalized Born and surface area continuum solvation (MM/GBSA) method or the molecular mechanics Poisson-Boltzmann surface area (MM/PBSA) approach, after transforming the CHARMM psf topology files to an Amber prmtop format using ParmEd (documentation at <http://parmed.github.io/ParmEd/html/index.html).

Supplementary Videos were produced employing VMD and avconv (at https://libav.org/avconv.html). Molecular graphics images were produced using the UCSF Chimera[121] (v1.14).

**Numbering system**

Throughout the manuscript, the Ballesteros-Weinstein residues numbering system for class A[122] and the Wootten residues numbering system for class B GPCRs[123] are adopted.

## ASSOCIATED CONTENT

Supporting Information (PDF)

Supporting Videos S1-S8 (mpg).

All the MD trajectories (stripped of POPC, water molecules, and ions) and topology files (psf and pdb) are available here:

https://zenodo.org/record/7944479

The mwSuMD software version used in this study is available at:

https://github.com/pipitoludovico/mwSuMD

### Author Contributions

GD and CAR conceived and supervised the project; GD designed and implemented the software and planned the simulations; GD, LP, RMR, TW, and PG carried out the simulations; GD analyzed the data; GD, AC, SM, and CAR interpreted the results, GD wrote the manuscript with input from CAR, AC, and SM; all the authors edited and reviewed the final version of the manuscript.

### Acknowledgments
GD is a member of the GPCRs-focused European COST action ERNEST. CAR is grateful for a Royal Society Industry Fellowship. GD and CAR are grateful for support from the BBSRC (BB/W016974/1) and from Diabetes UK (BDA 20/0006307).

### Competing Interest
All authors declare that they have no conflicts of interest.

Bibliography


(1) Cuzzolin, A.; Sturlese, M.; Deganutti, G.; Salmaso, V.; Sabbadin, D.; Ciancetta, A.; Moro, S. Deciphering the Complexity of Ligand-Protein Recognition Pathways Using Supervised Molecular Dynamics (SuMD) Simulations. *J. Chem. Inf. Model.* **2016**, *56*, 687–705.

(2) Deganutti, G.; Moro, S.; Reynolds, C. A. A Supervised Molecular Dynamics Approach to Unbiased Ligand-Protein Unbinding. *J. Chem. Inf. Model.* **2020**, *60*, 1804–1817.

(3) de Mendoza, A.; Sebé-Pedrós, A.; Ruiz-Trillo, I. The Evolution of the GPCR Signaling System in Eukaryotes: Modularity, Conservation, and the Transition to Metazoan Multicellularity. *Genome Biol. Evol.* **2014**, *6*, 606–619.

(4) Sriram, K.; Insel, P. A. G Protein-Coupled Receptors as Targets for Approved Drugs: How Many Targets and How Many Drugs? *Mol. Pharmacol.* **2018**, *93*, 251–258.

(5) Schiöth, H. B.; Fredriksson, R. The GRAFS Classification System of G-Protein Coupled Receptors in Comparative Perspective. *Gen. Comp. Endocrinol.* **2005**, *142*, 94–101.

(6) G protein-coupled receptors | G protein-coupled receptors | IUPHAR/BPS Guide to PHARMACOLOGY https://www.guidetopharmacology.org/GRAC/FamilyDisplayForward?familyId=694 (accessed May 18, 2022).

(7) Syrovatkina, V.; Alegre, K. O.; Dey, R.; Huang, X.-Y. Regulation, Signaling, and Physiological Functions of G-Proteins. *J. Mol. Biol.* **2016**, *428*, 3850–3868.

(8) Tan, L.; Yan, W.; McCorvy, J. D.; Cheng, J. Biased Ligands of G Protein-Coupled Receptors (GPCRs): Structure-Functional Selectivity Relationships (SFSRs) and Therapeutic Potential. *J. Med. Chem.* **2018**, *61*, 9841–9878.

(9) Flock, T.; Hauser, A. S.; Lund, N.; Gloriam, D. E.; Balaji, S.; Babu, M. M. Selectivity Determinants of GPCR-G-Protein Binding. *Nature* **2017**, *545*, 317–322.

(10) Hollingsworth, S. A.; Dror, R. O. Molecular Dynamics Simulation for All. *Neuron* **2018**, *99*, 1129–1143.

(11) Durrant, J. D.; McCammon, J. A. Molecular Dynamics Simulations and Drug Discovery. *BMC Biol.* **2011**, *9*, 71.

(12) Bussi, G.; Laio, A. Using Metadynamics to Explore Complex Free-Energy Landscapes. *Nat. Rev. Phys.* **2020**.

(13) Hamelberg, D.; Mongan, J.; McCammon, J. A. Accelerated Molecular Dynamics: A Promising and Efficient Simulation Method for Biomolecules. *J. Chem. Phys.* **2004**, *120*, 11919–11929.

(14) Miao, Y.; Feher, V. A.; McCammon, J. A. Gaussian Accelerated Molecular Dynamics: Unconstrained Enhanced Sampling and Free Energy Calculation. *J. Chem. Theory Comput.* **2015**, *11*, 3584–3595.

(15) Mattedi, G.; Acosta-Gutiérrez, S.; Clark, T.; Gervasio, F. L. A Combined Activation Mechanism for the Glucagon Receptor. *Proc. Natl. Acad. Sci. USA* **2020**.

(16) Miao, Y.; McCammon, J. A. Mechanism of the G-Protein Mimetic Nanobody Binding to a Muscarinic G-Protein-Coupled Receptor. *Proc. Natl. Acad. Sci. USA* **2018**, *115*, 3036–3041.

(17) Zuckerman, D. M.; Chong, L. T. Weighted Ensemble Simulation: Review of Methodology, Applications, and Software. *Annu. Rev. Biophys.* **2017**, *46*, 43–57.
(18) Sabbadin, D.; Moro, S. Supervised Molecular Dynamics (SuMD) as a Helpful Tool to Depict GPCR-Ligand Recognition Pathway in a Nanosecond Time Scale. *J. Chem. Inf. Model.* **2014**, *54*, 372–376.
(19) Deganutti, G.; Atanasio, S.; Rujan, R.-M.; Sexton, P. M.; Wootten, D.; Reynolds, C. A. Exploring Ligand Binding to Calcitonin Gene-Related Peptide Receptors. *Front. Mol. Biosci.* **2021**, *8*, 720561.
(20) Dong, M.; Deganutti, G.; Piper, S. J.; Liang, Y.-L.; Khoshouei, M.; Belousoff, M. J.; Harikumar, K. G.; Reynolds, C. A.; Glukhova, A.; Furness, S. G. B.; Christopoulos, A.; Danev, R.; Wootten, D.; Sexton, P. M.; Miller, L. J. Structure and Dynamics of the Active Gs-Coupled Human Secretin Receptor. *Nat. Commun.* **2020**, *11*, 4137.
(21) Deganutti, G.; Prischi, F.; Reynolds, C. A. Supervised Molecular Dynamics for Exploring the Druggability of the SARS-CoV-2 Spike Protein. *J. Comput. Aided Mol. Des.* **2021**, *35*, 195–207.
(22) Cary, B. P.; Deganutti, G.; Zhao, P.; Truong, T. T.; Piper, S. J.; Liu, X.; Belousoff, M. J.; Danev, R.; Sexton, P. M.; Wootten, D.; Gellman, S. H. Structural and Functional Diversity among Agonist-Bound States of the GLP-1 Receptor. *Nat. Chem. Biol.* **2021**.
(23) Wall, M. J.; Hill, E.; Huckstepp, R.; Barkan, K.; Deganutti, G.; Leuenberger, M.; Preti, B.; Winfield, I.; Carvalho, S.; Suchankova, A.; Wei, H.; Safitri, D.; Huang, X.; Imlach, W.; La Mache, C.; Dean, E.; Hume, C.; Hayward, S.; Oliver, J.; Zhao, F.-Y.; Spanswick, D.; Reynolds, C. A.; Lochner, M.; Ladds, G.; Frenguelli, B. G. Selective Activation of Gαob by an Adenosine A1 Receptor Agonist Elicits Analgesia without Cardiorespiratory Depression. *Nat. Commun.* **2022**, *13*, 4150.
(24) Culhane, K. J.; Gupte, T. M.; Madhugiri, I.; Gadgil, C. J.; Sivaramakrishnan, S. Kinetic Model of GPCR-G Protein Interactions Reveals Allokairic Modulation of Signaling. *Nat. Commun.* **2022**, *13*, 1202.
(25) Guo, D.; Heitman, L. H.; IJzerman, A. P. Kinetic Aspects of the Interaction between Ligand and G Protein-Coupled Receptor: The Case of the Adenosine Receptors. *Chem. Rev.* **2017**, *117*, 38–66.
(26) Guo, D.; Heitman, L. H.; IJzerman, A. P. The Role of Target Binding Kinetics in Drug Discovery. *ChemMedChem* **2015**, *10*, 1793–1796.
(27) Canals, M.; Marcellino, D.; Fanelli, F.; Ciruela, F.; de Benedetti, P.; Goldberg, S. R.; Neve, K.; Fuxe, K.; Agnati, L. F.; Woods, A. S.; Ferré, S.; Lluis, C.; Bouvier, M.; Franco, R. Adenosine A2A-Dopamine D2 Receptor-Receptor Heteromerization: Qualitative and Quantitative Assessment by Fluorescence and Bioluminescence Energy Transfer. *J. Biol. Chem.* **2003**, *278*, 46741–46749.
(28) Fuxe, K.; Guidolin, D.; Agnati, L. F.; Borroto-Escuela, D. O. Dopamine Heteroreceptor Complexes as Therapeutic Targets in Parkinson's Disease. *Expert Opin. Ther. Targets* **2015**, *19*, 377–398.
(29) Rivera-Oliver, M.; Díaz-Ríos, M. Using Caffeine and Other Adenosine Receptor Antagonists and Agonists as Therapeutic Tools against Neurodegenerative Diseases: A Review. *Life Sci.* **2014**, *101*, 1–9.
(30) Richardson, P. J.; Kase, H.; Jenner, P. G. Adenosine A2A Receptor Antagonists as New Agents for the Treatment of Parkinson's Disease.

*Trends Pharmacol. Sci.* **1997**, *18*, 338–344.
(31) Fuxe, K.; Borroto-Escuela, D. O. Heteroreceptor Complexes and Their Allosteric Receptor-Receptor Interactions as a Novel Biological Principle for Integration of Communication in the CNS: Targets for Drug Development. *Neuropsychopharmacology* **2016**, *41*, 380–382.
(32) Soriano, A.; Ventura, R.; Molero, A.; Hoen, R.; Casadó, V.; Cortés, A.; Fanelli, F.; Albericio, F.; Lluís, C.; Franco, R.; Royo, M. Adenosine A2A Receptor-Antagonist/Dopamine D2 Receptor-Agonist Bivalent Ligands as Pharmacological Tools to Detect A2A-D2 Receptor Heteromers. *J. Med. Chem.* **2009**, *52*, 5590–5602.
(33) Pulido, D.; Casadó-Anguera, V.; Gómez-Autet, M.; Llopart, N.; Moreno, E.; Casajuana-Martin, N.; Ferré, S.; Pardo, L.; Casadó, V.; Royo, M. Heterobivalent Ligand for the Adenosine A2A-Dopamine D2 Receptor Heteromer. *J. Med. Chem.* **2022**.
(34) Birnbaumer, M. Vasopressin Receptors. *Trends Endocrinol. Metab.* **2000**, *11*, 406–410.
(35) Ball, S. G. Vasopressin and Disorders of Water Balance: The Physiology and Pathophysiology of Vasopressin. *Ann Clin Biochem* **2007**, *44*, 417–431.
(36) Gioia, D.; Bertazzo, M.; Recanatini, M.; Masetti, M.; Cavalli, A. Dynamic Docking: A Paradigm Shift in Computational Drug Discovery. *Molecules* **2017**, *22*.
(37) Isberg, V.; Mordalski, S.; Munk, C.; Rataj, K.; Harpsøe, K.; Hauser, A. S.; Vroling, B.; Bojarski, A. J.; Vriend, G.; Gloriam, D. E. GPCRdb: An Information System for G Protein-Coupled Receptors. *Nucleic Acids Res.* **2016**, *44*, D356-64.
(38) Atanasio, S.; Deganutti, G.; Reynolds, C. A. Addressing Free Fatty Acid Receptor 1 (FFAR1) Activation Using Supervised Molecular Dynamics. *J. Comput. Aided Mol. Des.* **2020**, *34*, 1181–1193.
(39) Deganutti, G.; Barkan, K.; Preti, B.; Leuenberger, M.; Wall, M.; Frenguelli, B. G.; Lochner, M.; Ladds, G.; Reynolds, C. A. Deciphering the Agonist Binding Mechanism to the Adenosine A1 Receptor. *ACS Pharmacol. Transl. Sci.* **2021**, *4*, 314–326.
(40) Deganutti, G.; Barkan, K.; Ladds, G.; Reynolds, C. A. A Multisite Model of Allosterism for the Adenosine A1 Receptor. *BioRxiv* **2020**.
(41) Rasmussen, S. G. F.; DeVree, B. T.; Zou, Y.; Kruse, A. C.; Chung, K. Y.; Kobilka, T. S.; Thian, F. S.; Chae, P. S.; Pardon, E.; Calinski, D.; Mathiesen, J. M.; Shah, S. T. A.; Lyons, J. A.; Caffrey, M.; Gellman, S. H.; Steyaert, J.; Skiniotis, G.; Weis, W. I.; Sunahara, R. K.; Kobilka, B. K. Crystal Structure of the B2 Adrenergic Receptor-Gs Protein Complex. *Nature* **2011**, *477*, 549–555.
(42) Liang, Y.-L.; Belousoff, M. J.; Fletcher, M. M.; Zhang, X.; Khoshouei, M.; Deganutti, G.; Koole, C.; Furness, S. G. B.; Miller, L. J.; Hay, D. L.; Christopoulos, A.; Reynolds, C. A.; Danev, R.; Wootten, D.; Sexton, P. M. Structure and Dynamics of Adrenomedullin Receptors AM1 and AM2 Reveal Key Mechanisms in the Control of Receptor Phenotype by Receptor Activity-Modifying Proteins. *ACS Pharmacol. Transl. Sci.* **2020**, *3*, 263–284.
(43) Masuho, I.; Kise, R.; Gainza, P.; Von Moo, E.; Li, X.; Tany, R.; Wakasugi-Masuho, H.; Correia, B. E.; Martemyanov, K. A. Rules and Mechanisms Governing G Protein Coupling Selectivity of GPCRs. *Cell Rep.* **2023**, *42*, 113173.

(44) Linder, M. E.; Middleton, P.; Hepler, J. R.; Taussig, R.; Gilman, A. G.; Mumby, S. M. Lipid Modifications of G Proteins: Alpha Subunits Are Palmitoylated. *Proc. Natl. Acad. Sci. USA* **1993**, *90*, 3675–3679.
(45) Zhang, Z.; Melia, T. J.; He, F.; Yuan, C.; McGough, A.; Schmid, M. F.; Wensel, T. G. How a G Protein Binds a Membrane. *J. Biol. Chem.* **2004**, *279*, 33937–33945.
(46) Li, Y.; Sun, J.; Li, D.; Lin, J. The Full Activation Mechanism of the Adenosine A1 Receptor Revealed by GaMD and Su-GaMD Simulations. *Proc. Natl. Acad. Sci. USA* **2022**, *119*, e2203702119.
(47) Zhao, P.; Liang, Y.-L.; Belousoff, M. J.; Deganutti, G.; Fletcher, M. M.; Willard, F. S.; Bell, M. G.; Christe, M. E.; Sloop, K. W.; Inoue, A.; Truong, T. T.; Clydesdale, L.; Furness, S. G. B.; Christopoulos, A.; Wang, M.-W.; Miller, L. J.; Reynolds, C. A.; Danev, R.; Sexton, P. M.; Wootten, D. Activation of the GLP-1 Receptor by a Non-Peptidic Agonist. *Nature* **2020**, *577*, 432–436.
(48) Kawai, T.; Sun, B.; Yoshino, H.; Feng, D.; Suzuki, Y.; Fukazawa, M.; Nagao, S.; Wainscott, D. B.; Showalter, A. D.; Droz, B. A.; Kobilka, T. S.; Coghlan, M. P.; Willard, F. S.; Kawabe, Y.; Kobilka, B. K.; Sloop, K. W. Structural Basis for GLP-1 Receptor Activation by LY3502970, an Orally Active Nonpeptide Agonist. *Proc. Natl. Acad. Sci. USA* **2020**, *117*, 29959–29967.
(49) Ma, H.; Huang, W.; Wang, X.; Zhao, L.; Jiang, Y.; Liu, F.; Guo, W.; Sun, X.; Zhong, W.; Yuan, D.; Xu, H. E. Structural Insights into the Activation of GLP-1R by a Small Molecule Agonist. *Cell Res.* **2020**, *30*, 1140–1142.
(50) Zhang, X.; Belousoff, M. J.; Zhao, P.; Kooistra, A. J.; Truong, T. T.; Ang, S. Y.; Underwood, C. R.; Egebjerg, T.; Šenel, P.; Stewart, G. D.; Liang, Y.-L.; Glukhova, A.; Venugopal, H.; Christopoulos, A.; Furness, S. G. B.; Miller, L. J.; Reedtz-Runge, S.; Langmead, C. J.; Gloriam, D. E.; Danev, R.; Sexton, P. M.; Wootten, D. Differential GLP-1R Binding and Activation by Peptide and Non-Peptide Agonists. *Mol. Cell* **2020**, *80*, 485–500.e7.
(51) Cong, Z.; Chen, L.-N.; Ma, H.; Zhou, Q.; Zou, X.; Ye, C.; Dai, A.; Liu, Q.; Huang, W.; Sun, X.; Wang, X.; Xu, P.; Zhao, L.; Xia, T.; Zhong, W.; Yang, D.; Eric Xu, H.; Zhang, Y.; Wang, M.-W. Molecular Insights into Ago-Allosteric Modulation of the Human Glucagon-like Peptide-1 Receptor. *Nat. Commun.* **2021**, *12*, 3763.
(52) Cong, Z.; Zhou, Q.; Li, Y.; Chen, L.-N.; Zhang, Z.-C.; Liang, A.; Liu, Q.; Wu, X.; Dai, A.; Xia, T.; Wu, W.; Zhang, Y.; Yang, D.; Wang, M.-W. Structural Basis of Peptidomimetic Agonism Revealed by Small Molecule GLP-1R Agonists Boc5 and WB4-24. *BioRxiv* **2022**.
(53) Cong, Z.; Liang, Y.-L.; Zhou, Q.; Darbalaei, S.; Zhao, F.; Feng, W.; Zhao, L.; Xu, H. E.; Yang, D.; Wang, M.-W. Structural Perspective of Class B1 GPCR Signaling. *Trends Pharmacol. Sci.* **2022**, *43*, 321–334.
(54) Zhang, X.; Johnson, R. M.; Drulyte, I.; Yu, L.; Kotecha, A.; Danev, R.; Wootten, D.; Sexton, P. M.; Belousoff, M. J. Evolving Cryo-EM Structural Approaches for GPCR Drug Discovery. *Structure* **2021**, *29*, 963–974.e6.
(55) Ibrahim, P.; Wifling, D.; Clark, T. Universal Activation Index for Class A Gpcrs. *J. Chem. Inf. Model.* **2019**, *59*, 3938–3945.
(56) Deganutti, G.; Liang, Y.-L.; Zhang, X.; Khoshouei, M.; Clydesdale, L.; Belousoff, M. J.; Venugopal, H.; Truong, T. T.; Glukhova, A.; Keller, A. N.; Gregory, K. J.; Leach, K.; Christopoulos, A.; Danev, R.; Reynolds, C. A.; Zhao, P.; Sexton, P. M.; Wootten, D. Dynamics of GLP-1R Peptide Agonist Engagement Are Correlated with Kinetics of G Protein Activation. *Nat.*

*Commun.* **2022**, *13*, 92.
(57) Gregorio, G. G.; Masureel, M.; Hilger, D.; Terry, D. S.; Juette, M.; Zhao, H.; Zhou, Z.; Perez-Aguilar, J. M.; Hauge, M.; Mathiasen, S.; Javitch, J. A.; Weinstein, H.; Kobilka, B. K.; Blanchard, S. C. Single-Molecule Analysis of Ligand Efficacy in B2AR-G-Protein Activation. *Nature* **2017**, *547*, 68–73.
(58) Dror, R. O.; Mildorf, T. J.; Hilger, D.; Manglik, A.; Borhani, D. W.; Arlow, D. H.; Philippsen, A.; Villanueva, N.; Yang, Z.; Lerch, M. T.; Hubbell, W. L.; Kobilka, B. K.; Sunahara, R. K.; Shaw, D. E. SIGNAL TRANSDUCTION. Structural Basis for Nucleotide Exchange in Heterotrimeric G Proteins. *Science* **2015**, *348*, 1361–1365.
(59) Sun, X.; Singh, S.; Blumer, K. J.; Bowman, G. R. Simulation of Spontaneous G Protein Activation Reveals a New Intermediate Driving GDP Unbinding. *Elife* **2018**, *7*.
(60) Kaya, A. I.; Lokits, A. D.; Gilbert, J. A.; Iverson, T. M.; Meiler, J.; Hamm, H. E. A Conserved Hydrophobic Core in Gαi1 Regulates G Protein Activation and Release from Activated Receptor. *J. Biol. Chem.* **2016**, *291*, 19674–19686.
(61) Flock, T.; Ravarani, C. N. J.; Sun, D.; Venkatakrishnan, A. J.; Kayikci, M.; Tate, C. G.; Veprintsev, D. B.; Babu, M. M. Universal Allosteric Mechanism for Gα Activation by GPCRs. *Nature* **2015**, *524*, 173–179.
(62) Borroto-Escuela, D. O.; Rodriguez, D.; Romero-Fernandez, W.; Kapla, J.; Jaiteh, M.; Ranganathan, A.; Lazarova, T.; Fuxe, K.; Carlsson, J. Mapping the Interface of a GPCR Dimer: A Structural Model of the A2A Adenosine and D2 Dopamine Receptor Heteromer. *Front. Pharmacol.* **2018**, *9*, 829.
(63) Ramadurai, S.; Holt, A.; Krasnikov, V.; van den Bogaart, G.; Killian, J. A.; Poolman, B. Lateral Diffusion of Membrane Proteins. *J. Am. Chem. Soc.* **2009**, *131*, 12650–12656.
(64) Dickson, A.; Brooks, C. L. WExplore: Hierarchical Exploration of High-Dimensional Spaces Using the Weighted Ensemble Algorithm. *J. Phys. Chem. B* **2014**, *118*, 3532–3542.
(65) Sugita, Y.; Okamoto, Y. Replica-Exchange Molecular Dynamics Method for Protein Folding. *Chem. Phys. Lett.* **1999**, *314*, 141–151.
(66) Wang, E.; Sun, H.; Wang, J.; Wang, Z.; Liu, H.; Zhang, J. Z. H.; Hou, T. End-Point Binding Free Energy Calculation with MM/PBSA and MM/GBSA: Strategies and Applications in Drug Design. *Chem. Rev.* **2019**, *119*, 9478–9508.
(67) Vögler, O.; Barceló, J. M.; Ribas, C.; Escribá, P. V. Membrane Interactions of G Proteins and Other Related Proteins. *Biochim. Biophys. Acta* **2008**, *1778*, 1640–1652.
(68) Stanley, N.; Pardo, L.; Fabritiis, G. D. The Pathway of Ligand Entry from the Membrane Bilayer to a Lipid G Protein-Coupled Receptor. *Sci. Rep.* **2016**, *6*, 22639.
(69) Bokoch, M. P.; Jo, H.; Valcourt, J. R.; Srinivasan, Y.; Pan, A. C.; Capponi, S.; Grabe, M.; Dror, R. O.; Shaw, D. E.; DeGrado, W. F.; Coughlin, S. R. Entry from the Lipid Bilayer: A Possible Pathway for Inhibition of a Peptide G Protein-Coupled Receptor by a Lipophilic Small Molecule. *Biochemistry* **2018**.
(70) Yuan, S.; Xia, L.; Wang, C.; Wu, F.; Zhang, B.; Pan, C.; Fan, Z.; Lei, X.; Stevens, R. C.; Sali, A.; Sun, L.; Shui, W. Conformational Dynamics of the Activated GLP-1 Receptor-$G_s$ Complex Revealed by Cross-Linking Mass Spectrometry and Integrative Structure Modeling. *ACS Cent. Sci.* **2023**.

(71) Goddard, A. D.; Dijkman, P. M.; Adamson, R. J.; Watts, A. Lipid-Dependent GPCR Dimerization. *Methods Cell Biol.* **2013**, *117*, 341–357.
(72) Prasanna, X.; Sengupta, D.; Chattopadhyay, A. Cholesterol-Dependent Conformational Plasticity in GPCR Dimers. *Sci. Rep.* **2016**, *6*, 31858.
(73) Meng, X.-Y.; Mezei, M.; Cui, M. Computational Approaches for Modeling GPCR Dimerization. *Curr. Pharm. Biotechnol.* **2014**, *15*, 996–1006.
(74) Pérez de Alba Ortíz, A.; Vreede, J.; Ensing, B. The Adaptive Path Collective Variable: A Versatile Biasing Approach to Compute the Average Transition Path and Free Energy of Molecular Transitions. *Methods Mol. Biol.* **2019**, *2022*, 255–290.
(75) Husic, B. E.; Pande, V. S. Markov State Models: From an Art to a Science. *J. Am. Chem. Soc.* **2018**, *140*, 2386–2396.
(76) Kokh, D. B.; Kaufmann, T.; Kister, B.; Wade, R. C. Machine Learning Analysis of TRAMD Trajectories to Decipher Molecular Determinants of Drug-Target Residence Times. *Front. Mol. Biosci.* **2019**, *6*, 36.
(77) Pérez, A.; Martínez-Rosell, G.; De Fabritiis, G. Simulations Meet Machine Learning in Structural Biology. *Curr. Opin. Struct. Biol.* **2018**, *49*, 139–144.
(78) Harvey, M. J.; Giupponi, G.; Fabritiis, G. D. ACEMD: Accelerating Biomolecular Dynamics in the Microsecond Time Scale. *J. Chem. Theory Comput.* **2009**, *5*, 1632–1639.
(79) Phillips, J. C.; Braun, R.; Wang, W.; Gumbart, J.; Tajkhorshid, E.; Villa, E.; Chipot, C.; Skeel, R. D.; Kalé, L.; Schulten, K. Scalable Molecular Dynamics with NAMD. *J. Comput. Chem.* **2005**, *26*, 1781–1802.
(80) Berendsen, H. J. C.; van der Spoel, D.; van Drunen, R. GROMACS: A Message-Passing Parallel Molecular Dynamics Implementation. *Comput Phys Commun* **1995**, *91*, 43–56.
(81) Eastman, P.; Swails, J.; Chodera, J. D.; McGibbon, R. T.; Zhao, Y.; Beauchamp, K. A.; Wang, L.-P.; Simmonett, A. C.; Harrigan, M. P.; Stern, C. D.; Wiewiora, R. P.; Brooks, B. R.; Pande, V. S. OpenMM 7: Rapid Development of High Performance Algorithms for Molecular Dynamics. *PLoS Comput. Biol.* **2017**, *13*, e1005659.
(82) Deganutti, G.; Moro, S. Estimation of Kinetic and Thermodynamic Ligand-Binding Parameters Using Computational Strategies. *Future Med. Chem.* **2017**, *9*, 507–523.
(83) Salmaso, V.; Sturlese, M.; Cuzzolin, A.; Moro, S. Exploring Protein-Peptide Recognition Pathways Using a Supervised Molecular Dynamics Approach. *Structure* **2017**, *25*, 655–662.e2.
(84) Bower, R. L.; Yule, L.; Rees, T. A.; Deganutti, G.; Hendrikse, E. R.; Harris, P. W. R.; Kowalczyk, R.; Ridgway, Z.; Wong, A. G.; Swierkula, K.; Raleigh, D. P.; Pioszak, A. A.; Brimble, M. A.; Reynolds, C. A.; Walker, C. S.; Hay, D. L. Molecular Signature for Receptor Engagement in the Metabolic Peptide Hormone Amylin. *ACS Pharmacol. Transl. Sci.* **2018**, *1*, 32–49.
(85) Michaud-Agrawal, N.; Denning, E. J.; Woolf, T. B.; Beckstein, O. MDAnalysis: A Toolkit for the Analysis of Molecular Dynamics Simulations. *J. Comput. Chem.* **2011**, *32*, 2319–2327.
(86) McGibbon, R. T.; Beauchamp, K. A.; Harrigan, M. P.; Klein, C.; Swails, J. M.; Hernández, C. X.; Schwantes, C. R.; Wang, L.-P.; Lane, T. J.; Pande, V. S. Mdtraj: A Modern Open Library for the Analysis of Molecular Dynamics Trajectories. *Biophys. J.* **2015**, *109*, 1528–1532.
(87) Huang, J.; MacKerell, A. D. CHARMM36 All-Atom Additive Protein Force

Field: Validation Based on Comparison to NMR Data. *J. Comput. Chem.* **2013**, *34*, 2135–2145.
(88) Huang, J.; Rauscher, S.; Nawrocki, G.; Ran, T.; Feig, M.; de Groot, B. L.; Grubmüller, H.; MacKerell, A. D. CHARMM36m: An Improved Force Field for Folded and Intrinsically Disordered Proteins. *Nat. Methods* **2017**, *14*, 71–73.
(89) Vanommeslaeghe, K.; MacKerell, A. D. Automation of the CHARMM General Force Field (CGenFF) I: Bond Perception and Atom Typing. *J. Chem. Inf. Model.* **2012**, *52*, 3144–3154.
(90) Vanommeslaeghe, K.; Raman, E. P.; MacKerell, A. D. Automation of the CHARMM General Force Field (CGenFF) II: Assignment of Bonded Parameters and Partial Atomic Charges. *J. Chem. Inf. Model.* **2012**, *52*, 3155–3168.
(91) Yu, W.; He, X.; Vanommeslaeghe, K.; MacKerell, A. D. Extension of the CHARMM General Force Field to Sulfonyl-Containing Compounds and Its Utility in Biomolecular Simulations. *J. Comput. Chem.* **2012**, *33*, 2451–2468.
(92) Woods, R. J.; Chappelle, R. Restrained Electrostatic Potential Atomic Partial Charges for Condensed-Phase Simulations of Carbohydrates. *Theochem* **2000**, *527*, 149–156.
(93) Dolinsky, T. J.; Nielsen, J. E.; McCammon, J. A.; Baker, N. A. PDB2PQR: An Automated Pipeline for the Setup of Poisson-Boltzmann Electrostatics Calculations. *Nucleic Acids Res.* **2004**, *32*, W665-7.
(94) Olsson, M. H. M.; Søndergaard, C. R.; Rostkowski, M.; Jensen, J. H. PROPKA3: Consistent Treatment of Internal and Surface Residues in Empirical PK Predictions. *J. Chem. Theory Comput.* **2011**, *7*, 525–537.
(95) Sommer, B. Membrane Packing Problems: A Short Review on Computational Membrane Modeling Methods and Tools. *Comput Struct Biotechnol J* **2013**, *5*, e201302014.
(96) Lomize, M. A.; Lomize, A. L.; Pogozheva, I. D.; Mosberg, H. I. OPM: Orientations of Proteins in Membranes Database. *Bioinformatics* **2006**, *22*, 623–625.
(97) Jorgensen, W. L.; Chandrasekhar, J.; Madura, J. D.; Impey, R. W.; Klein, M. L. Comparison of Simple Potential Functions for Simulating Liquid Water. *J. Chem. Phys.* **1983**, *79*, 926.
(98) Berendsen, H. J. C.; Postma, J. P. M.; van Gunsteren, W. F.; DiNola, A.; Haak, J. R. Molecular Dynamics with Coupling to an External Bath. *J. Chem. Phys.* **1984**, *81*, 3684.
(99) Loncharich, R. J.; Brooks, B. R.; Pastor, R. W. Langevin Dynamics of Peptides: The Frictional Dependence of Isomerization Rates of N-Acetylalanyl-N'-Methylamide. *Biopolymers* **1992**, *32*, 523–535.
(100) Forester, T. R.; Smith, W. SHAKE, Rattle, and Roll: Efficient Constraint Algorithms for Linked Rigid Bodies. *J. Comput. Chem.* **1998**.
(101) Krautler, V.; van Gunsteren, W. F.; Hunenberger, P. H. A Fast SHAKE Algorithm to Solve Distance Constraint Equations for Small Molecules in Molecular Dynamics Simulations. *J. Comput. Chem.* **2001**, *22*, 501–508.
(102) Essmann, U.; Perera, L.; Berkowitz, M. L.; Darden, T.; Lee, H.; Pedersen, L. G. A Smooth Particle Mesh Ewald Method. *J. Chem. Phys.* **1995**, *103*, 8577.
(103) Zhou, F.; Ye, C.; Ma, X.; Yin, W.; Croll, T. I.; Zhou, Q.; He, X.; Zhang, X.; Yang, D.; Wang, P.; Xu, H. E.; Wang, M.-W.; Jiang, Y. Molecular Basis of Ligand Recognition and Activation of Human V2 Vasopressin Receptor. *Cell Res.* **2021**, *31*, 929–931.

(104) Berman, H. M.; Westbrook, J.; Feng, Z.; Gilliland, G.; Bhat, T. N.; Weissig, H.; Shindyalov, I. N.; Bourne, P. E. The Protein Data Bank. *Nucleic Acids Res.* **2000**, *28*, 235–242.
(105) Fiser, A.; Sali, A. Modeller: Generation and Refinement of Homology-Based Protein Structure Models. *Meth. Enzymol.* **2003**, *374*, 461–491.
(106) Ring, A. M.; Manglik, A.; Kruse, A. C.; Enos, M. D.; Weis, W. I.; Garcia, K. C.; Kobilka, B. K. Adrenaline-Activated Structure of B2-Adrenoceptor Stabilized by an Engineered Nanobody. *Nature* **2013**, *502*, 575–579.
(107) Liu, X.; Xu, X.; Hilger, D.; Aschauer, P.; Tiemann, J. K. S.; Du, Y.; Liu, H.; Hirata, K.; Sun, X.; Guixà-González, R.; Mathiesen, J. M.; Hildebrand, P. W.; Kobilka, B. K. Structural Insights into the Process of GPCR-G Protein Complex Formation. *Cell* **2019**, *177*, 1243–1251.e12.
(108) Jumper, J.; Evans, R.; Pritzel, A.; Green, T.; Figurnov, M.; Ronneberger, O.; Tunyasuvunakool, K.; Bates, R.; Žídek, A.; Potapenko, A.; Bridgland, A.; Meyer, C.; Kohl, S. A. A.; Ballard, A. J.; Cowie, A.; Romera-Paredes, B.; Nikolov, S.; Jain, R.; Adler, J.; Back, T.; Petersen, S.; Reiman, D.; Clancy, E.; Zielinski, M.; Steinegger, M.; Pacholska, M.; Berghammer, T.; Bodenstein, S.; Silver, D.; Vinyals, O.; Senior, A. W.; Kavukcuoglu, K.; Kohli, P.; Hassabis, D. Highly Accurate Protein Structure Prediction with AlphaFold. *Nature* **2021**, *596*, 583–589.
(109) Jo, S.; Kim, T.; Iyer, V. G.; Im, W. CHARMM-GUI: A Web-Based Graphical User Interface for CHARMM. *J. Comput. Chem.* **2008**, *29*, 1859–1865.
(110) Mystek, P.; Rysiewicz, B.; Gregrowicz, J.; Dziedzicka-Wasylewska, M.; Polit, A. Gγ and Gα Identity Dictate a G-Protein Heterotrimer Plasma Membrane Targeting. *Cells* **2019**, *8*.
(111) Wu, F.; Yang, L.; Hang, K.; Laursen, M.; Wu, L.; Han, G. W.; Ren, Q.; Roed, N. K.; Lin, G.; Hanson, M. A.; Jiang, H.; Wang, M.-W.; Reedtz-Runge, S.; Song, G.; Stevens, R. C. Full-Length Human GLP-1 Receptor Structure without Orthosteric Ligands. *Nat. Commun.* **2020**, *11*, 1272.
(112) Mayne, C. G.; Saam, J.; Schulten, K.; Tajkhorshid, E.; Gumbart, J. C. Rapid Parameterization of Small Molecules Using the Force Field Toolkit. *J. Comput. Chem.* **2013**, *34*, 2757–2770.
(113) Weinert, T.; Olieric, N.; Cheng, R.; Brünle, S.; James, D.; Ozerov, D.; Gashi, D.; Vera, L.; Marsh, M.; Jaeger, K.; Dworkowski, F.; Panepucci, E.; Basu, S.; Skopintsev, P.; Doré, A. S.; Geng, T.; Cooke, R. M.; Liang, M.; Prota, A. E.; Panneels, V.; Nogly, P.; Ermler, U.; Schertler, G.; Hennig, M.; Steinmetz, M. O.; Wang, M.; Standfuss, J. Serial Millisecond Crystallography for Routine Room-Temperature Structure Determination at Synchrotrons. *Nat. Commun.* **2017**, *8*, 542.
(114) Fan, L.; Tan, L.; Chen, Z.; Qi, J.; Nie, F.; Luo, Z.; Cheng, J.; Wang, S. Haloperidol Bound D2 Dopamine Receptor Structure Inspired the Discovery of Subtype Selective Ligands. *Nat. Commun.* **2020**, *11*, 1074.
(115) Marchi, M.; Ballone, P. Adiabatic Bias Molecular Dynamics: A Method to Navigate the Conformational Space of Complex Molecular Systems. *J. Chem. Phys.* **1999**, *110*, 3697.
(116) Laio, A.; Parrinello, M. Escaping Free-Energy Minima. *Proc. Natl. Acad. Sci. USA* **2002**, *99*, 12562–12566.
(117) Barducci, A.; Bussi, G.; Parrinello, M. Well-Tempered Metadynamics: A Smoothly Converging and Tunable Free-Energy Method. *Phys. Rev. Lett.* **2008**, *100*, 020603.

(118) Tribello, G. A.; Bonomi, M.; Branduardi, D.; Camilloni, C.; Bussi, G. PLUMED 2: New Feathers for an Old Bird. *Comput Phys Commun* **2014**, *185*, 604–613.
(119) Humphrey, W.; Dalke, A.; Schulten, K. VMD: Visual Molecular Dynamics. *J Mol Graph* **1996**, *14*, 33–38, 27.
(120) Miller, B. R.; McGee, T. D.; Swails, J. M.; Homeyer, N.; Gohlke, H.; Roitberg, A. E. MMPBSA.Py: An Efficient Program for End-State Free Energy Calculations. *J. Chem. Theory Comput.* **2012**, *8*, 3314–3321.
(121) Pettersen, E. F.; Goddard, T. D.; Huang, C. C.; Couch, G. S.; Greenblatt, D. M.; Meng, E. C.; Ferrin, T. E. UCSF Chimera—a Visualization System for Exploratory Research and Analysis. *J. Comput. Chem.* **2004**, *25*, 1605–1612.
(122) Ballesteros, J. A.; Weinstein, H. [19] Integrated Methods for the Construction of Three-Dimensional Models and Computational Probing of Structure-Function Relations in G Protein-Coupled Receptors. In *Receptor Molecular Biology*; Methods in Neurosciences; Elsevier, 1995; Vol. 25, pp. 366–428.
(123) Wootten, D.; Simms, J.; Miller, L. J.; Christopoulos, A.; Sexton, P. M. Polar Transmembrane Interactions Drive Formation of Ligand-Specific and Signal Pathway-Biased Family B G Protein-Coupled Receptor Conformations. *Proc. Natl. Acad. Sci. USA* **2013**, *110*, 5211–5216.